

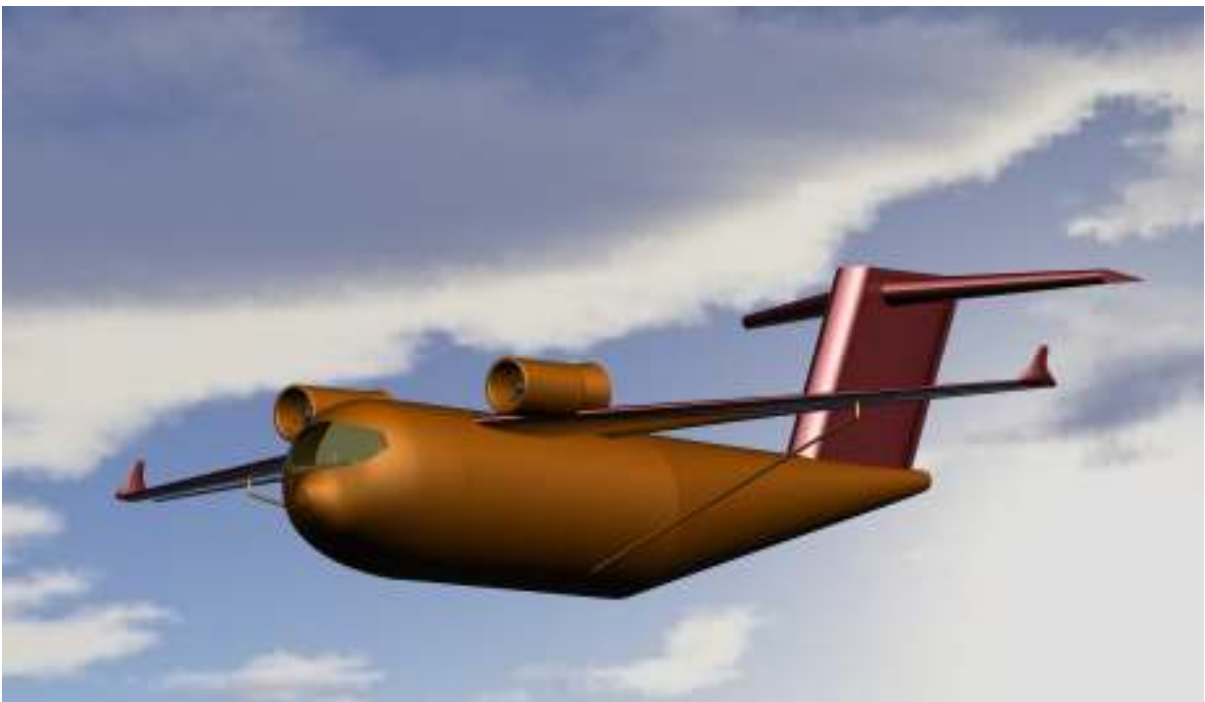
Response to the 2006-2007 AIAA Undergraduate
Team Aircraft Design Competition



PRESENTS

Hermes

An Inter-theater Tactical STOL Transport



Virginia Polytechnic Institute and State University
Aerospace Engineering Department
Blacksburg, Virginia
Spring 2007



Team Roster

Member	AIAA Number	Signature
Robert Adams	279075	<i>Lee Adams</i>
Ryan Arnaudin	235266	<i>Ryan Arnaudin</i>
LaMar Berry	279849	<i>LaMar J. Berry</i>
Shelley Biagi	274326	<i>Shelley Biagi</i>
William Black	281932	<i>W. Curtis Black</i>
Angela Brooks	277820	<i>Angela Brooks</i>
Steven Brusco	281931	<i>Steven Brusco</i>
Nicholas Carlson	266422	<i>Nicholas Carlson</i>
Faculty Advisor		
Dr. William H. Mason		

Executive Summary

Arrowspace is proud to announce Hermes, a Short Takeoff and Landing (STOL) tactical transport aircraft with austere theatre capability. Hermes is designed to meet the 2006-2007 AIAA Competition Request for Proposal (RFP). Hermes is a twin engine tactical STOL transport aircraft capable of delivering the Stryker, the Future Deployable Armored Vehicle (FDAV) specified in the RFP, or 30 tons of payloads anywhere within a 600 nautical mile mission radius. This aircraft employs an upper surface blowing engine configuration mounted on high strut-braced wings to achieve short take off and landing (STOL) in austere environments. The engines used on this design are 80% scaled AIAA engines with a high bypass ratio of 6, mounted above and slightly forward of the wings in a USB configuration. The interior of the plane is designed to carry the Stryker, 3 crew members, and any necessary support equipment. This design also allows for a 3200 nm trans-oceanic ferry mission with 10 tons of payloads and can be modified for civilian use if the need arises. By incorporating advanced technology into the aircraft's avionics and communication systems, Hermes will directly integrate into current and rising combat support systems.

Hermes was designed to out perform all current US Military transport aircraft by being able to simultaneously achieve STOL and cruise efficiently at or above 80% Mach. By meeting these requirements, Hermes is able to fulfill the ever increasing mission demands essential to carry out US military operations.

The ability for a transport to accomplish both low speed performance and control while retaining a transonic cruise capability is a valued asset in today's global theatre. Achieving these contradictory goals over the timeline of the Hermes conceptual design proved difficult. The process involved balancing low weight and cost while trying to incorporate and exploit several advanced technologies to achieve our design goal. Specifically, this involved producing a design that can efficiently cruise while retaining the ability for above average field performance. This versatility is no longer just desired, but is demanded by the needs associated with quick deployment to austere environments.

Advanced technologies played an invaluable role in our design. A powerful and efficient upper surface blowing engine configuration makes the most of current high-lift technologies. Integrating the engine set-up, while preserving the required trim during flight, proved tricky because there are few flying examples with the Hermes' configuration. To enhance the potential of Hermes, struts were incorporated

into the concept. Although struts further add to the overall complexity, the benefits outweigh this fact if integrated correctly. Advanced systems were incorporated into the design to attain the highest level of survivability, while simultaneously remaining feasible. Composite materials are built into Hermes structure to keep weight as low as possible.

Several key aspects of our advanced technologies proved hard to quantify in our preliminary analyses. Key assumptions were made in lieu of this; numerous studies and research projects provided reliable estimates of design implications. For example, predicting the change in span loading as a consequence of upper surface blowing was difficult to determine in the absence of experimental tests. Evaluating the efficiency of our high lift system was another major uncertainty in the design. Analytically estimating the drag on our aerodynamic configuration proved more difficult without the results from a wind-tunnel.

Table of Contents

Executive Summary	3
Index of Tables	7
Index of Figures	8
Index of Acronyms	9
Index of Symbols	10
1 Introduction and RFP Requirements	11
1.1 Introduction.....	11
1.2 RFP Analysis	11
1.3 Challenges associated with RFP	12
2 Design Drivers.....	13
3 Design Concepts.....	14
3.1 Introduction.....	14
3.2 Common Design Considerations	14
3.2.1 Payload and Crew Location	14
3.2.2 Landing Gear Configuration	15
3.3 Tri-Engine Design	15
3.4 Blended Wing Body.....	16
3.5 Hermes Design.....	17
3.6 Pros and Cons	18
4 Sizing Hermes	19
4.1 Summary of Design	19
4.2 Initial Sizing.....	19
4.2.1 Evaluating Sizing Constraints	23
4.2.2 Improving the Design Point	24
4.3 Design Sketch	25
5 Configuration	26
5.1 Fuselage	30
5.2 Wings and Engines	31
5.3 Cargo Bay and Tail Assembly	31
5.4 Cockpit.....	32
5.5 Landing Gear	33
5.6 Upper Surface Blowing	34
6 Weight and CG Analysis	35
6.1 Component Weights	35
6.2 Center of Gravity	37
7 Aerodynamics.....	38
7.1 Wing Planform.....	38
7.2 Airfoil Selection.....	40
7.3 Wing Analysis	44
7.4 High Lift Selection.....	45
7.4.1 Spanload Distribution.....	47
7.5 Drag.....	48
7.5.1 Drag Breakdown	48
7.5.2 Drag Polar	51
8 Propulsion	54
8.1 Engine Configuration and Selection	54
8.2 Inlet and Nacelle Sizing	57
8.3 Exit Nozzle	57
8.4 Engine Removal and Maintenance	59
8.5 Noise.....	60
8.6 Additional Features.....	60
9 Stability and Control	62
9.1 Tail Sizing.....	62

9.2	Control Surface Sizing.....	63
9.3	Longitudinal Static Stability.....	65
9.4	Lateral/Directional Static Stability.....	66
9.5	Dynamic Stability.....	67
9.6	Flight Control Systems.....	68
9.7	AVL Model and Assumptions.....	69
10	Materials and Structures.....	72
10.1	Materials.....	72
10.2	Weight Reduction.....	73
10.3	Struts.....	73
10.4	Wings.....	75
10.5	Fuselage.....	76
10.6	V-n Diagram.....	78
11	Systems.....	80
11.1	Cockpit.....	81
11.2	Lighting.....	82
11.3	Fuel System.....	83
11.4	Landing Gear.....	84
11.5	Shrink Shock Strut Summary.....	85
12	Hermes Performance.....	86
12.1	Mission Program and Design Adjustments.....	86
12.1	Take-Off and Landing.....	87
12.2	Climb and Ceiling.....	90
12.3	Performance Summary.....	90
13	Cost Estimation.....	93
13.1	Flyaway and Life Cycle Cost Estimation.....	93
13.2	Cost Sensitivities.....	95
	References.....	96

Index of Tables

Table 2-1: Comparator Matrix	13
Table 4-1: Fuel Fractions	21
Table 4-2: Weight Estimation	22
Table 6-1: Weights and CG for Primary and Secondary Missions	36
Table 7-1: Planform Parameters	40
Table 7-2: Airfoils Tested in TSfoil.....	41
Table 7-3: Zero-Lift Drag Buildup for Take Off	49
Table 7-4: Zero-Lift Drag Buildup for Cruise	49
Table 7-5: Zero-Lift Drag Buildup for Landing	50
Table 7-6: Total Drag Buildup.....	50
Table 8-1: Engine Sizing	56
Table 9-1: Flight Conditions	62
Table 9-2: Wing and Tail Characteristics	63
Table 9-3: Wing Control Surfaces	64
Table 9-4: Tail Control Surfaces.....	65
Table 9-5: Longitudinal Stability and Control Derivatives.....	66
Table 9-6: Lateral/Directional Stability and Control Derivatives	67
Table 9-7: Dimensional Stability Derivatives.....	68
Table 9-8: Hermes 3-D	71
Table 10-1: Materials (27, 13, 32, 29)	72
Table 10-2: Weight Reduction Numbers	73
Table 12-1: Hermes Landing Distances.....	89
Table 12-2: Climb Parameters	90
Table 12-3: Comparator Aircraft	91
Table 12-4: Hermes' Performance Summary	92
Table 13-1: Main Inputs for Flyaway Cost Estimation.....	94
Table 13-2: Flyaway Cost Estimation.....	94
Table 13-3: Life Cycle Cost Estimation	95
Table 13-4: Cost Sensitivities	95

Index of Figures

Figure 3-1: Orthographic drawing of the Tri-Engine concept	16
Figure 3-2: Orthographic drawing of the Blended-Wing Body concept	17
Figure 3-3: Orthographic drawing of Hermes concept	18
Figure 4-1: Primary Mission Profile	20
Figure 4-2: Secondary Mission Profile	20
Figure 4-3: Preliminary Sizing Constraints	23
Figure 4-4: Hermes Rendered	25
Figure 5-1: Hermes 3-D View	27
Figure 5-2: Hermes Inboard Profile	28
Figure 5-3: Hermes Isometric View	29
Figure 5-4: Hermes Fuselage	30
Figure 5-5: Close-up of Hermes Engine and Wing	31
Figure 5-6: Rear View of Hermes Cargo Bay and Tail Assembly	32
Figure 5-7: Close-up View of Hermes Cockpit	33
Figure 5-8: Close-up View of Hermes Landing Gear	34
Figure 6-1: Center of Gravity Travel for Different Phases	37
Figure 7-1: Planform Geometries	39
Figure 7-2: Wing Planform	40
Figure 7-3: Pressure Distribution for SC(2)-0412, SC(2)-0610, SC(2)-0710	42
Figure 7-4: The SC(2)-0710 Airfoil	42
Figure 7-5: Section Lift Curve Slope	43
Figure 7-6: Pressure Distribution at Cruise Conditions	44
Figure 7-7: Location of Wing on Fuselage	44
Figure 7-8: Lift Coefficient for Takeoff, Landing and Cruise	45
Figure 7-9: Section Lift Curves with High Lift	46
Figure 7-10: Hermes Wing Twist Selection	47
Figure 7-11: Drag Buildup at Cruise	51
Figure 7-12: Drag Polar for Take Off	52
Figure 7-13: Drag Polar for Cruise	52
Figure 7-14: Drag Polar for Landing	53
Figure 8-1: Engine Map for a Pair of AIAA Engines at Full Power	56
Figure 8-2: Cutaway View of Engine and Nacelle Layout	57
Figure 8-3: Overhead View of Exhaust Nozzle with Fully Extended Side Flaps	58
Figure 8-4: Rear View of Hermes' 3.5 Aspect Ratio D-nozzle	59
Figure 8-5: Engine Removal Method	60
Figure 8-6: Top View of Vortex Generators on Wing Surface	61
Figure 9-1: Wing Planform Control Surfaces	64
Figure 9-2: Hermes 3-D	69
Figure 10-1: Wing and Strut	74
Figure 10-2: Wing Section	75
Figure 10-3: Wing box	76
Figure 10-4: Fuselage stringers, skin, and pressure bulkhead	76
Figure 10-5: Fuselage (topview)	77
Figure 10-6: Fuselage (sideview)	77
Figure 10-7: V-n diagram for Hermes	79
Figure 11-1: Cockpit in Hermes aircraft	81
Figure 11-2: Hermes lighting configuration	83
Figure 11-3: Hermes main landing gear	84
Figure 12-1: Primary Mission Fuel Breakdown	87
Figure 12-2: Hermes TO and Balance Field Lengths	88

Index of Acronyms

AEO	All Engines Operating
AIAA	American Institute of Aeronautics and Astronautics
AR	Aspect Ratio
BWB	Blended Wing Body
CBR	California Bearing Ratio
CEI	Critical Engine Inoperative
CG	Center of Gravity
FDAV	Future Deployable Armor Vehicle
EMI	Electromagnetic Interference
JKay VLM	J Kay Vortex Lattice Method Fortran Program
MAC	Mean Aerodynamic Chord
NP	Neutral Point
QSRA	Quiet Short-Haul Research Aircraft
RFP	Request for Proposal
SAS	Stability Augmentation System
SAGAS	Stability Augmentation and Gust Alleviation System
STOL	Short takeoff and landing
TOGW	Take off gross weight
USB	Upper surface blowing

Index of Symbols

Symbol	Definition	Units
AR	Aspect Ratio	---
b	Span	ft
c	Volume Coefficient	---
C	Mean Chord Length	ft
C_d	Total drag	---
C_{d0}	Parasite drag	---
C_{Lmax}	Maximum lift coefficient	---
C_L	Lift coefficient	---
C_m	Moment Coefficient	---
$C_{L\alpha}$	Aircraft lift curve slope	/rad
C_{Lq}	Lift due to pitch rate derivative	/rad
C_{mq}	Pitching moment due to pitch rate derivative	/rad
C_{lp}	Rolling moment due to roll rate derivative	/rad
C_{np}	Yawing moment due to roll rate derivative	/rad
C_{lr}	Rolling moment due to yaw rate derivative	/rad
C_{nr}	Yawing moment due to yaw rate derivative	/rad
C_{yr}	Side force due to yaw rate derivative	/rad
$C_{l\beta}$	Rolling Moment due to Sideslip Coefficient	/rad
$C_{n\beta}$	Yawing Moment due to Sideslip Coefficient	/rad
$C_{y\beta}$	Side Force due to Sideslip Coefficient	/rad
$C_{l\delta a}$	Rolling moment due to aileron deflection derivative	/rad
$C_{n\delta a}$	Yawing moment due to aileron deflection derivative	/rad
$C_{L\delta e}$	Lift due to elevator deflection derivative	/rad
$C_{m\delta e}$	Pitching moment due to elevator deflection derivative/rad	
$C_{l\delta r}$	Rolling moment due to rudder deflection derivative	/rad
$C_{n\delta r}$	Yawing moment due to rudder deflection derivative	/rad
$C_{y\delta r}$	Side force due to rudder deflection derivative	/rad
e	Oswald efficiency factor	---
f	Parasite area	---
L	Lift	---
L_β	Roll moment due to sideslip	1/sec
L_r	Roll moment due to yaw rate	1/sec
M_α	Pitch moment due to angle of attack	1/sec ²
M_q	Pitch moment due to pitch rate	1/sec
N_β	Yaw moment due to sideslip	1/sec ²
N_r	Yaw moment due to yaw rate	1/sec
S_{ref}	Reference Surface Area	ft ²
S_{wet}	Wetted Surface Area	ft ²
S	Area	ft ²
t	Time	secs
t	Airfoil thickness	ft
T/W	Thrust to Weight Ratio	---
V	Velocity	ft/s
V_{Stall}	Stall Speed	ft/s
W	Weight	lbs
W_{TO}	Takeoff weight	lbs
Y_β	Side force moment due to sideslip	ft/sec ²
Y_r	Side force moment due to yaw rate	ft/sec
ρ	Density	slugs/ft ³

1 Introduction and RFP Requirements

1.1 Introduction

Transport aircraft have a long and well-known history of service within the U.S. military. For many years they have carried troops, equipment, and supplies to every corner of the world. While not directly involved in combat, their combat support role has been essential in deploying the U. S. military's power over time.

However, today's military transport aircraft are limited in their abilities to perform certain operations. Because of takeoff and landing requirements, they can only land in large areas with improved surfaces, usually far away from the battlefield. As the U.S. military continues to reshape itself for future combat, it will require transports that can take off and land in tighter areas with non-asphalt landing strips.

In addition, this new transport aircraft will also have to conduct peacetime operations acting as an overseas transport. This will be used to keep the military forces around the world in operational readiness at all times.

1.2 RFP Analysis

The AIAA RFP calls for an austere STOL transport to serve a primarily military function transporting a FDAV as directly as possible to the battle site. To compensate for the lack of control over the landing site, the transport must have the ability to land and take off within a 3,000 foot-long area with a California Bearing Ratio (CBR) between four and six. The transport must be able to fly to this site from a base 600 nm away, covering the first 500 nm at a best cruise altitude over 30,000 feet traveling at or above Mach 0.8. Then the transport must descend to 1,000 feet to cover the last 100 nm at a speed of Mach 0.6. It must be able to do all of this while carrying a 25-ton FDAV and 5 tons of support equipment. Upon delivery, the transport must then mirror its journey back to home base.

For its ferry mission, the transport must be able to carry 10 tons of equipment over a 3,200 nm range. The transport must travel at best cruise altitude above 30,000 feet while maintaining a speed at or above Mach 0.8, then land at the appropriate destination. In the event of a missed approach or unsuitable

landing conditions, the transport must hold enough fuel in order to divert to another landing site 150 nm away and keep a holding pattern for 45 minutes before landing.

1.3 Challenges associated with RFP

Rarely are the requirements of efficient transonic cruise and short-field take-off combined into one design. However, an aircraft that possess this sort of tactical flexibility is in high demand. In the context of aircraft design, these requirements do not cooperate well. An aircraft seeking to cruise transonically must have sufficient thrust and be streamlined aerodynamically to minimize drag. In terms of the aircraft, this usually corresponds to: a slender high aspect-ratio wing, high lift-to-drag configuration, and a minimized wetted area fuselage. In contrast, a STOL aircraft usually features relatively low wing-loading, highly cambered airfoils, and several mechanical or powered high lift features that create copious amounts of drag. The configuration of Hermes incorporates the required technologies to make both goals a reality.

2 Design Drivers

The main driver for this proposal was STOL capability. High subsonic cruise speed in the range of Mach 0.8, efficient cruise, low drag, and survivability were also of utmost importance. A study of comparator aircraft revealed that current tactical transports failed to meet either the RFP's requirements for STOL capability or cruise speed. As a result, three conceptual designs were studied for possible implementation in a final design that could meet these requirements. Each of these concepts attempted to meet the given requirements using advanced technologies. Upper surface blowing (USB), blown flaps, a blended wing-body configuration, and strut-braced wings were all studied for their ability to meet the requirements.

The overall design philosophy of Arrowspace entailed analyzing the requirements set forth in the RFP and then putting together three rough concepts. These three concepts were evaluated, mostly qualitatively, in the context of our requirements and constraints. Based off of how well these concepts met our design drivers, which are summarized in Table 2-1, a comparative chart was assembled for direct assessment of the conceptual designs and a decision was made. Following this decision, the details of the aircraft were hashed out and the performance was evaluated. This step was iterated over a majority of the conceptual design period. Table 2-1 shows a breakdown of our design drivers, how important each driver was to our selection of an aircraft concept, and Arrowspace's evaluation and subsequent recommendation.

	Weight	Hermes		Tri Engine		BWB	
TOGW	7	8	56	7	49	5	35
Cruise Efficiency	5	7	35	7	35	9	45
C_{Lmax}	6	9	54	7	42	9	54
L/D	3	8	24	8	24	9	27
TO & Landing Distance	8	9	72	8	64	5	40
Cost	1	8	8	8	8	4	4
Payload Integration	4	9	36	8	32	6	24
Survivability	2	8	16	8	16	6	12
Total			301		270		241

Table 2-1: Comparator Matrix

3 Design Concepts

3.1 Introduction

Three design concepts were chosen to meet the RFP goals of the 2006 AIAA design competition. The first concept chosen was a mid-wing, three engine design, the second concept was a blended-wing design, and the third concept was an USB strut-braced design. The three engine concept, or tri-engine concept, was chosen for its use of high sweep wings to achieve increased lift and fast takeoff. For the blended-wing concept, this design was chosen for its decreased fuselage drag and allows for more efficient flight performance in cruise. Hermes design was chosen for its upper surface blowing configuration and general sturdy design (strut-braced) which provides increased safety as well as good performance in engine out conditions. All three concepts and their respective orthographic drawings can be seen in the figures 3-1, 3-2, and 3-3.

3.2 Common Design Considerations

There were some basic parameters that were considered for all three designs. These basic considerations include payload and crew location, landing gear configuration and systems. These items will be discussed below.

3.2.1 Payload and Crew Location

In every concept it was envisioned that the crew quarters be located at the front of the aircraft. The payload would be positioned towards the aft part of the fuselage. However, when considering the payload location, the center of gravity of the aircraft must be accounted for also. If the payload was placed too far away from the center of gravity of the aircraft, tip-back could occur on the ground along with stability and control problems in the air. Therefore, the payload placement for all the concepts should be as close the center of gravity of the aircraft as possible. Since the center of gravity of aircraft is generally located in the general region of the wing location along the fuselage, it should be assumed that the payload

is placed as close to the wings as possible. This is an important reason to choose a wing carrythrough structure that uses as little fuselage space as possible.

3.2.2 Landing Gear Configuration

In all three design concepts a standard tricycle landing gear configuration would probably be the easiest and most efficient choice. However, with the blended-wing body concept an alternative landing gear configuration might be considered due to the large mass of the wing spread in the lateral direction which creates a need for either a wider tricycle landing gear placement or a new configuration all together. A detailed location for the landing gear placement is a complicated task for a blended wing aircraft and this complication takes time and money that cost points in the decision process.

With tricycle landing gear configuration chosen for the final design, then a vital decision must be made. It must be decided if the main landing gear (at the rear of the aircraft) should retract vertically or horizontally as it compares to the space allotted inside of the fuselage within this region. Obviously, the nose landing gear should retract either forward or backward as is almost standard with all aircraft.

3.3 Tri-Engine Design

The three engine or tri-engine concept makes use of two wing mounted engines and a single tail mounted engine which is expected to supply additional thrust needed for the short take off. This design also uses of a mid-wing configuration and is based on the fairly simple principle of creating more lift with the use of more lifting surfaces. In order for this specific configuration to work, the box carrythrough, which is common to high-speed transports and general aviation aircraft, would have to be disregarded for another carrythrough configuration that provides more space within the fuselage at the wing carrythrough area. Possible choices would be a ring-frame carrythrough structure that uses heavy bulkheads to carry the bending moment through the fuselage, or a bending beam carrythrough where the wing panels are attached to the side of the fuselage to carry the lift forces (ref. 30). A drawing of the concept is given in figure 3-1.

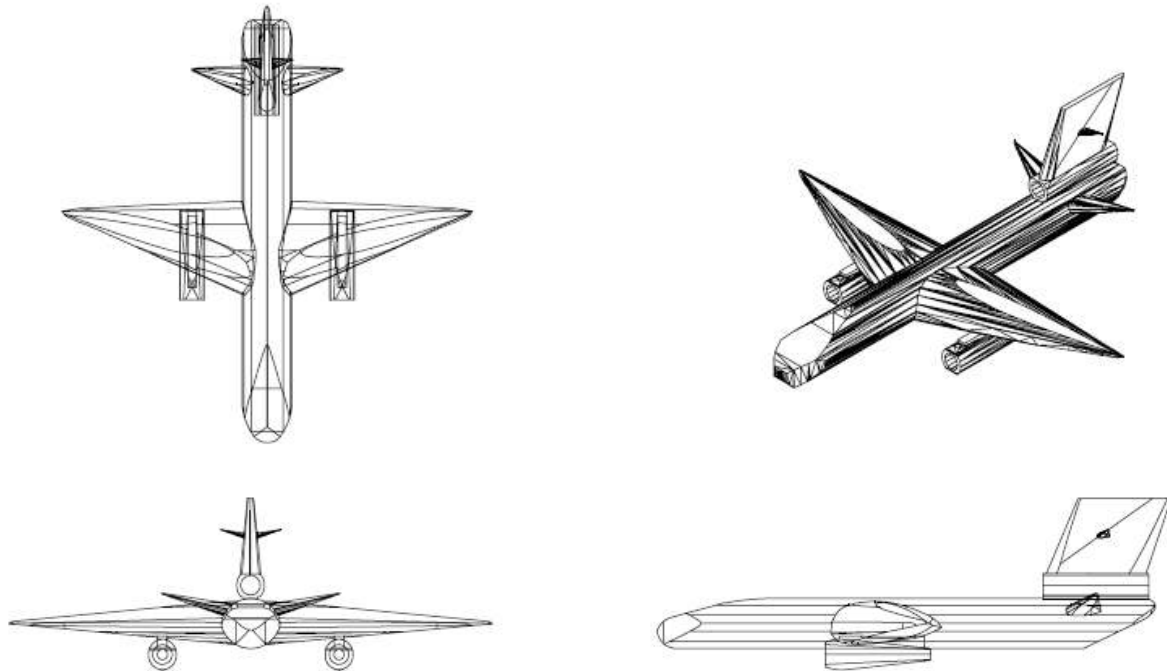


Figure 3-1: Orthographic drawing of the Tri-Engine concept

3.4 Blended Wing Body

Overall the blended-wing design is not an ideal STOL concept because of its inability for quick takeoff and landings due to the large wingspan and relatively low performance in optimal conditions. High angles of attack are also not obtainable during takeoff. However it was considered because of its efficient cruise that would allow for long-range hauls as prescribed by the secondary mission. For the blended wing-body concept a wing carrythrough structure would not have to be considered since the aircraft is essentially a flying wing. However, a structural analysis would be needed at the body-wing intersection points to examine the structural integrity of the area and determine if structural reinforcement would be needed. A drawing of the blended wing concept is given in figure 3-2.

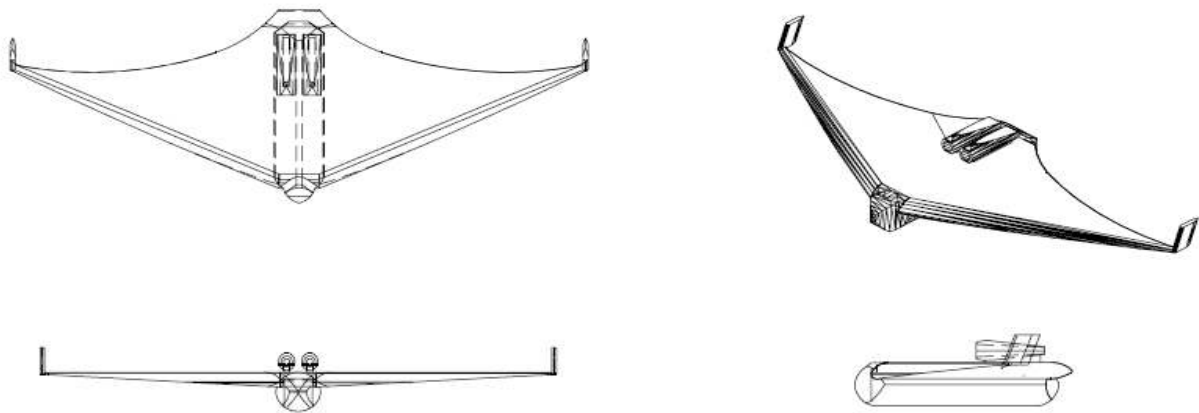


Figure 3-2: Orthographic drawing of the Blended-Wing Body concept

3.5 Hermes Design

The conventional concept was designed with two major elements in mind: upper surface blowing and strut-braced wings. Upper surface blowing would enhance the STOL capabilities of the aircraft with added lift at takeoff and the strut-braced wings would provide more structural support and increased space for payload in the fuselage and fuel in the wings. The conventional design makes use of a strut-braced carrythrough structure. This design allows for most of the fuselage volume to be used for carrying the payload. However, with increased useable fuselage volume, the drag penalty from the struts is significant at high speeds (ref. 30). Specifically, if the strut is oriented at an angle to the wing, a shock may occur at this intersection point in high speed flight conditions causing boundary layer separation and increased drag. An early drawing of Hermes is found in figure 3-3.

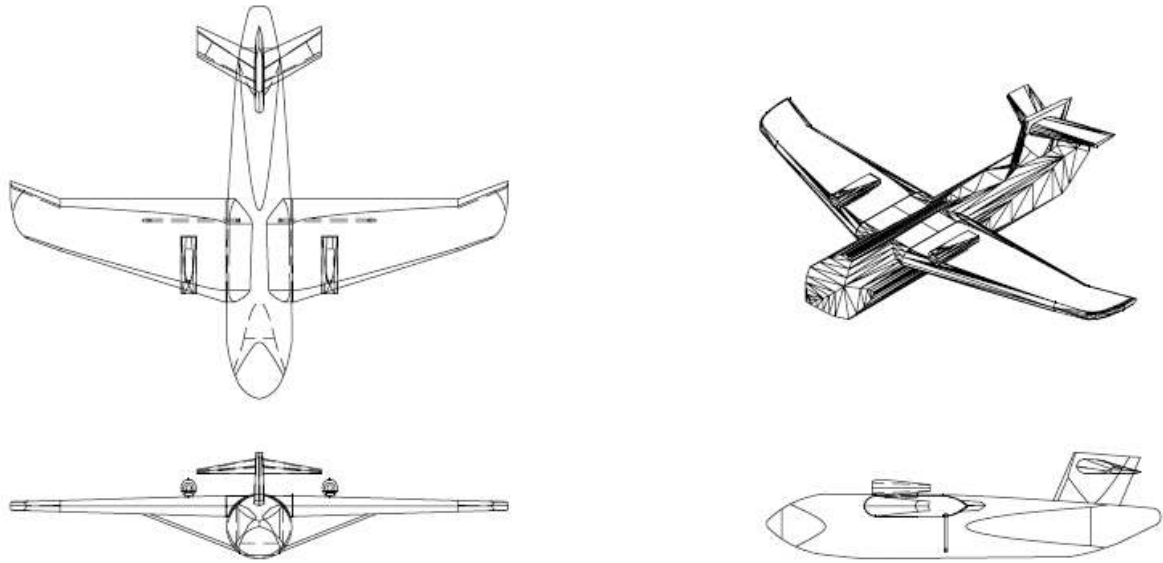


Figure 3-3: Orthographic drawing of Hermes concept

3.6 Pros and Cons

After careful consideration of the pros and cons of each design, a preferred design concept was chosen. Taking all the mission drivers and RFP requirements into consideration, it was concluded that the Hermes design with upper surface blowing was the best option for the given missions.

4 Sizing Hermes

4.1 Summary of Design

In terms of cruise performance, weight, and STOL capability, Arrowspace has decided to select the USB design with strut-braced wings, or, Hermes. After evaluating all concepts in each area (propulsion, aerodynamics, etc.) it was decided that the blended-wing body concept was all together impractical as a STOL aircraft because of the stability problems at high angles of attack at take-off. The tri-engine concept was more geared towards achieving an optimal cruise speed and not short field performance. Hermes includes proven design features from current aircraft as well as several superior technologies that are currently being incorporated into aircraft designs.

4.2 Initial Sizing

Having analyzed the RFP and determined what factors would drive this design and consequently shape our aircraft; the next step was to determine what constraints would be limiting. After clearly defining constraints for the diverse flight conditions required by the RFP, the preliminary concepts were then compared and matched to the constraints.

Before the concepts are discussed the sizing method deserves more attention. Sizing methods from Roskam (ref. 36) and Raymer (ref. 34) were combined to provide a general sizing for our aircraft design. The first step in sizing an aircraft is to have clearly defined a primary mission; with secondary missions also being considered in this phase. After the mission has been defined, it must be broken down into segments. Figures 4-1 and 4-2 illustrate the mission segments of both the primary and secondary missions.

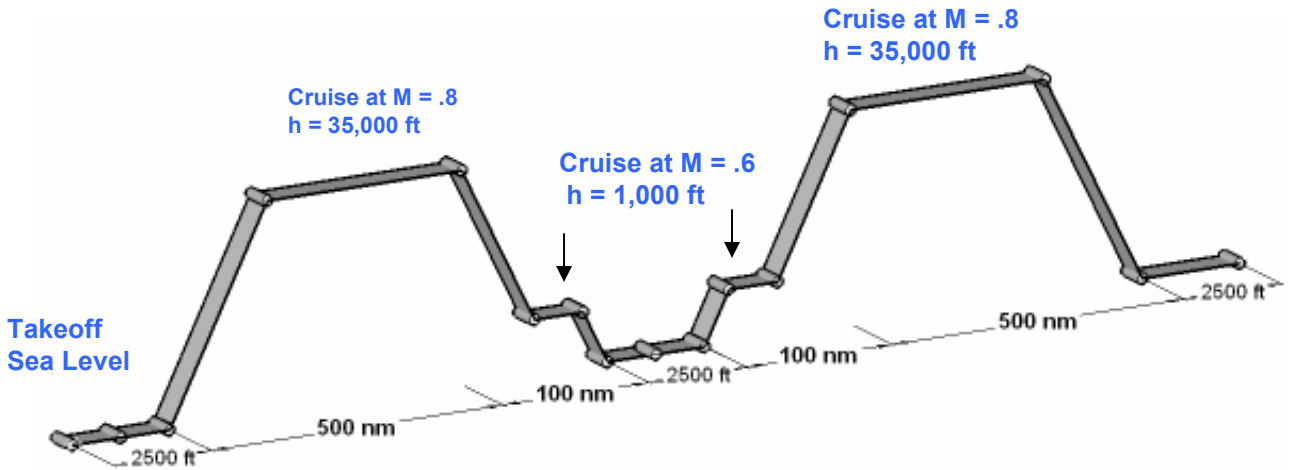


Figure 4-1: Primary Mission Profile

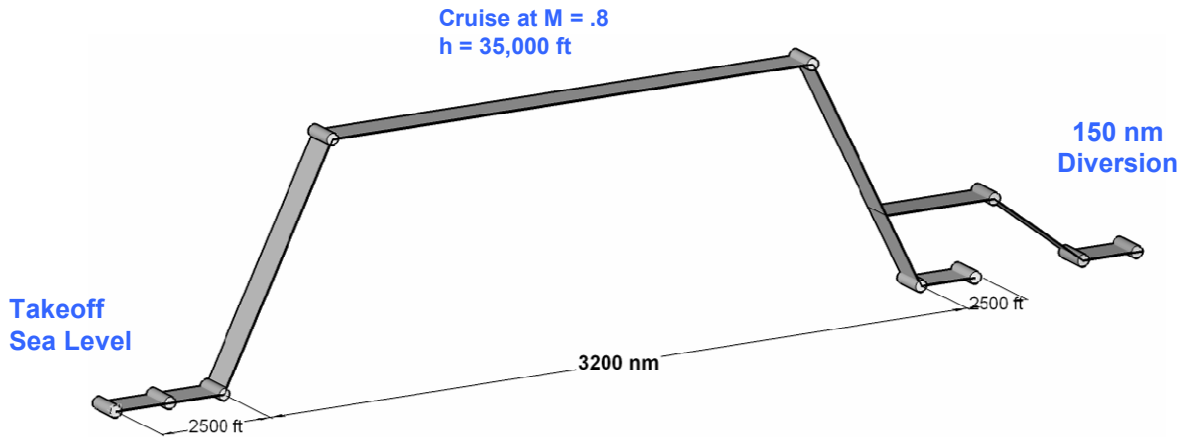


Figure 4-2: Secondary Mission Profile

With the mission now clearly defined, the overall mission fuel fraction was calculated. Fuel fractions represent a ratio of aircraft weight at the start and end of a mission segment, in terms of fuel used during the particular segment. Roskam provided a reliable estimate for fuel fractions during the warm-up, taxi, take-off, and climb segments of a military transport aircraft’s mission. However, estimates would not suffice for the cruise and vehicle deployment phases of the mission. The solution to this was to use Breguet’s range equation (ref. 36) to solve for the fuel fraction, given other parameters that are already defined. The final fuel fractions for the Primary Mission can be found in Table 4-1.

Table 4-1: Fuel Fractions

Mission Segment	Fuel Fraction
WarmUp/Taxi	0.98
Takeoff	0.995
Climb to Cruise	0.98
Cruise 500nm	0.9563
Mission 100nm	0.9887
Land/Deploy	0.985
Takeoff	0.995
Cruise 600nm	0.9478
Total Fuel Fraction	0.8393

The experienced designer will notice that the final mission fuel fraction is fairly high for a transport vehicle designed to drop a payload off and return. Since this is a military aircraft and the RFP calls for operation in an austere environment, it is entirely possible that this aircraft maybe be limited to not completing its mission. Taking this into consideration, the sizing was tailored such that enough fuel was allowed for the aircraft to safely return with the 60 ton cargo, should that be the scenario. Reserve and trapped fuel was calculated to increase the fuel requirement by 25.05% in our design. An iterative method, which compared empty weight required to an educated guess for Take-Off Gross Weight (TOGW), was used to calculate the TOGW. The sizing method provided in Roskam assumes aircraft construction with outdated materials, so to compensate for this, the author added empty weight adjustments based on more current aerospace materials and their corresponding weights. Reducing the empty weight also reduces the amount of fuel required for the mission. The results of the take-off weight sizing are:

Table 4-2: Weight Estimation

Take Off Weight Estimation (lbs)	
Iterated Take-off Weight	195500
Calculated Take-off Weight	195700
Empty Weight	94700
Equipment Weight Estimation	1500
Empty Weight with Reduction	80720
Original Fuel Weight	40180
Adjust Fuel Weight	36460
Adjusted Take-off Weight	177960

The design drivers were paramount in further sizing once we had a reliable TOGW calculated. Meeting the balanced field length of 2500 ft. was of primary concern; however, our aircraft will first have to meet Military and FAR Standards. Requirements considered at the preliminary design phase were basic climb and descent requirements for take-off and landing. For an engine-out (OEI) take-off, a climb gradient of 0.025 is required at the 50ft. obstacle, as defined in the RFP, and also at 115% of the stall speed. An engine-out landing requires a climb gradient of 0.025 over a 50 ft. landing obstacle. In the case that all engines are operating (AEO), which is hopefully the case 100% of the time, a climb gradient of 0.032 is required for landing in the event that there is an emergency and the aircraft has to take extreme measures. Roskam provided an equation that relates the climb gradient to the maximum lift-to-drag ratio required (ref. 36). These climb gradients were factored into the Preliminary Constraint Diagram (Figure 4-3), which served as our primary tool for size matching.

Using the take-off distance equation (ref. 36) a range of allowable thrust and wing loadings could be determined. It was cautioned by Roskam that this equation was derived for aircraft: experiencing little, to no, wind, taking off on a flat runway, and operating using conventional lifting devices. This equation was assumed approximate and reliable enough to base preliminary estimates off of. The approach speed, which can be represented as a multiple of stall speed, was used to help determine landing constraints. With the military approach defined as 120% of the aircraft's stall speed, the required wing loadings for landing can be computed as a function of the C_{Lmax} . Using the information from the estimated drag polar, having

been determined for the cruise condition already, a range of thrust and wing loadings can be found using a general performance equation found in Marchman's performance text (ref. 23), which is defined as a function of wing loading and thrust-to-weight ratio. The RFP required a minimum cruise Mach of 0.80 at best cruise altitude. We designed around this Mach number at a minimum cruise altitude of 35,000 ft. The results of the previous sizing constraints can be found on the Preliminary Constrain Diagram (Figure 4-3). The first-cut design point (red dot) corresponds to a wing loading of 75 psf and a thrust-to-weight ratio of roughly 0.35.

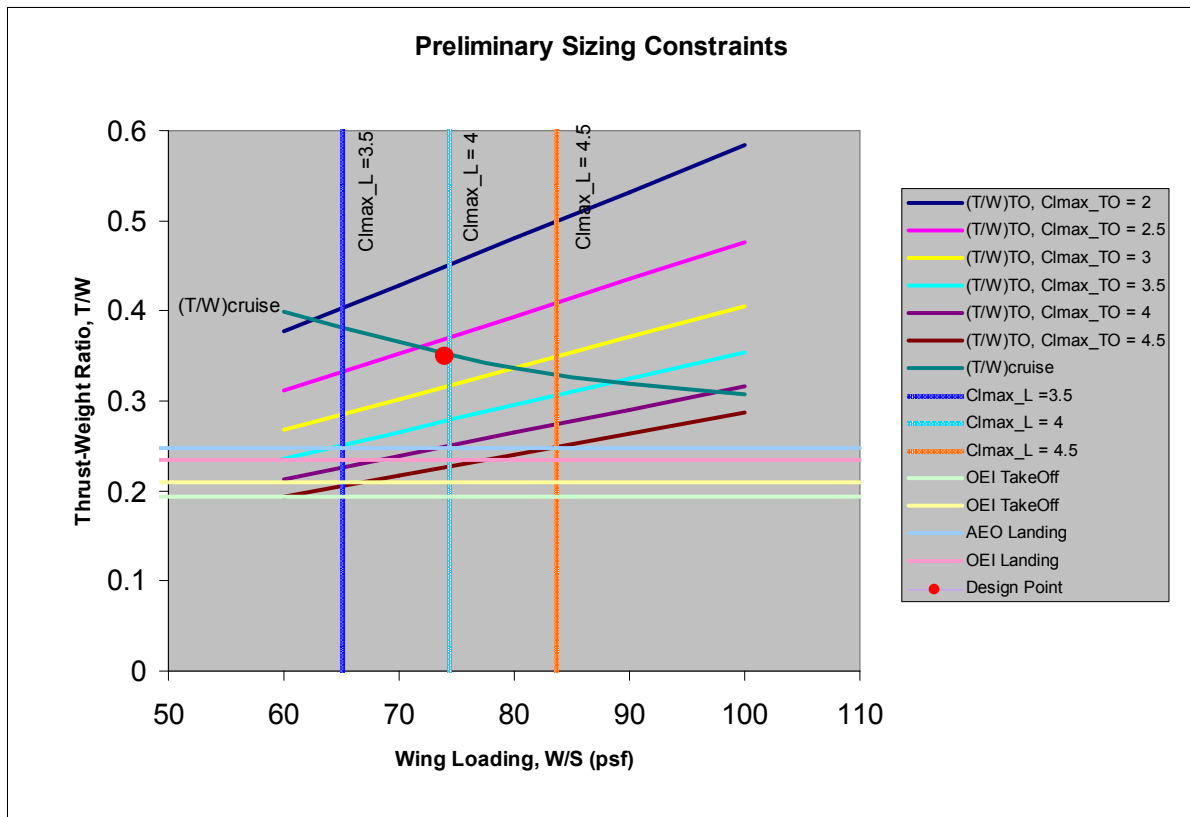


Figure 4-3: Preliminary Sizing Constraints

4.2.1 Evaluating Sizing Constraints

It was important to keep in mind that, when evaluating these constraints, the aircraft weight would constantly be changing during the mission phases. For example, meeting a wing loading requirement at take-off is different than needing to meet the same wing loading requirement at landing weight. Given our

constraints and initial sizing estimates it was evident that designing at the “saddle point”, or the intersection of the Take-off and Cruise curves, would not suffice for our requirements. A high C_{Lmax} is required for take-off, knowing that STOL is a main mission driver. It was estimated that a maximum lift-coefficient of around 4.5 would be need to meet the balanced field length requirement of 2,500 ft. Where this point would intersect the Cruise curve corresponds to a wing loading and thrust-weight ratio of roughly 97 lb/ft² and 0.31, respectively. These are undesirable numbers to design around for several reasons. For STOL operation, low wing loadings are desirable; the more wing you have, the quicker the take-off. Also, that specific thrust-weight ratio is not guaranteed to be sufficient for all of the mission requirements. Beyond the take-off problem, the current design point is on the wrong side of our landing constraint for $C_{Lmax} = 4.5$. At 97 lb/ft², there’s simply not enough wing area to create sufficient drag for our landing distance requirement of 2,500 ft.

4.2.2 Improving the Design Point

To better evaluate some performance parameters as they relate to our sizing constraints, a take-off and landing program was used to approximate take-off distances using only a few aircraft inputs. The take-off program represents the cumulative effort of each AIAA design group at Virginia Tech working together to improve an already accurate version that was previously published. The MATLAB® based program was converted from C++ then updated with better differential equation solvers. The new version also accounts for take-off at variable altitude-densities and wind gusts. For more information regarding the theory, assumptions, or approximations involved in developing the take-off program please reference Sean Lynn’s final report on his takeoff program (ref. 21).

There are infinitely many combinations of aircraft parameters that could lead to the required field performance. However, since there is a practical limit on C_{Lmax} that restricts take-off distance, values above 6.0 were not considered (ref. 17). Using the previously calculated TOGW estimate and the thrust available at sea level for both standard and hot conditions, it was determined the required wing loading and thrust-weight ratio required to meet the take-off requirement would be about 71 lb/ft² and 0.4, respectively. Previous take-off constraints were calculated with the assumption of mechanical flaps and no high-lift devices. If it is assumed that an effective C_{Lmax} increase of 2.5 can be provided by high-lift systems, then

our design point shifts to an acceptable point where all cruise, take-off, landing, and OEI constraints are met. These values were compared to or engine deck and our design concept values for a reality check. Figures 4-3 shows where the new design point falls within the constraints. For a target $C_{Lmax} \approx 4.5$ and wing loading between 70 and 75, a corresponding thrust of 43,000 lbs can be found. Checking in the AIAA engine decks, this thrust value is certainly achievable at sea level conditions.

4.3 Design Sketch



Figure 4-4: Hermes Rendered

5 Configuration

The basic design of Hermes is based on the original concept chosen in the conceptual design phase. Since the early design phase, the elements of the conventional concept have progressed into Hermes- a fully capable inter-theater tactical transport with austere STOL capability. Several views of Hermes are given in the following figures.

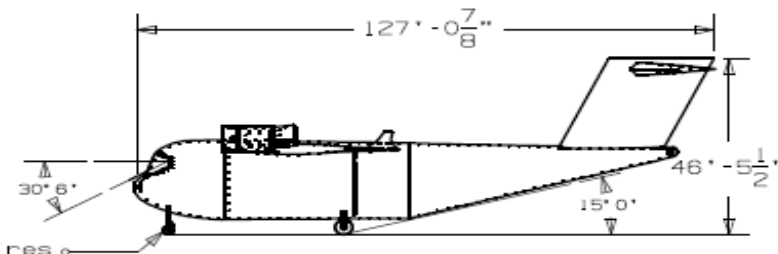
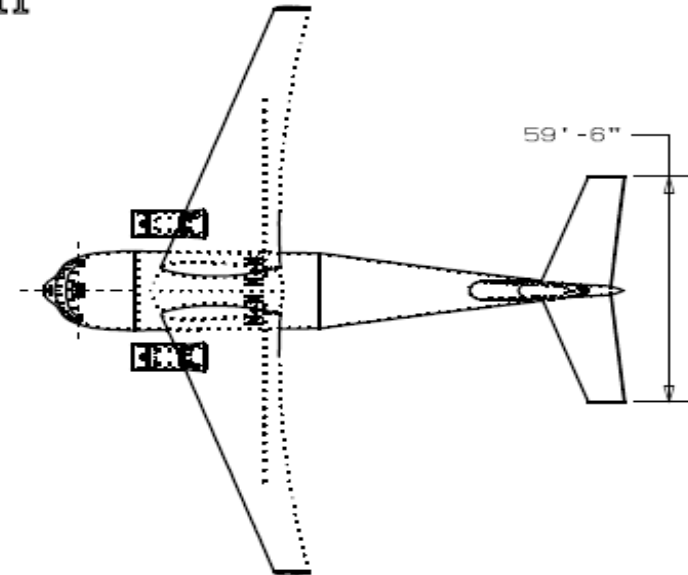
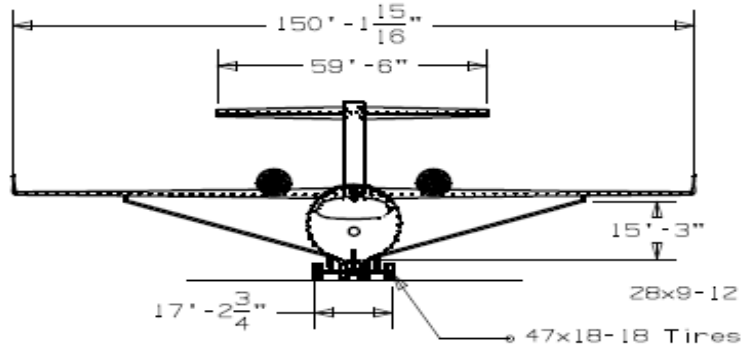
Hermes General Configuration

Geometry

	Wing	Horiz. Tail	Vert. Tail	
Airfoil	SC121-0710	NACA 0012	NACA 0013	
Area	2528	714.0	554.48	ft ²
Span	150	59.5	23.9	ft
Aspect Ratio	8.9	4.96	1.03	
Average Chord	16.1	12.0	23.2	ft
LE Sweep	20.14	20	25	deg
MAC	19.15	12.45	23.2	ft
MAC c/4	15.62	7.922	11.37	ft

Weights

Structures Group	58306.2	lbs
Propulsion Group	7594	lbs
Fuel System Group	616.3	lbs
Control Group	1572.4	lbs
Fixed Equipment Group	5684	lbs
Payload Group	97210	lbs



ARROWSPACE

General Arrangement

Date 5/04/07

Virginia Tech

Figure 5-1: Hermes 3-D View

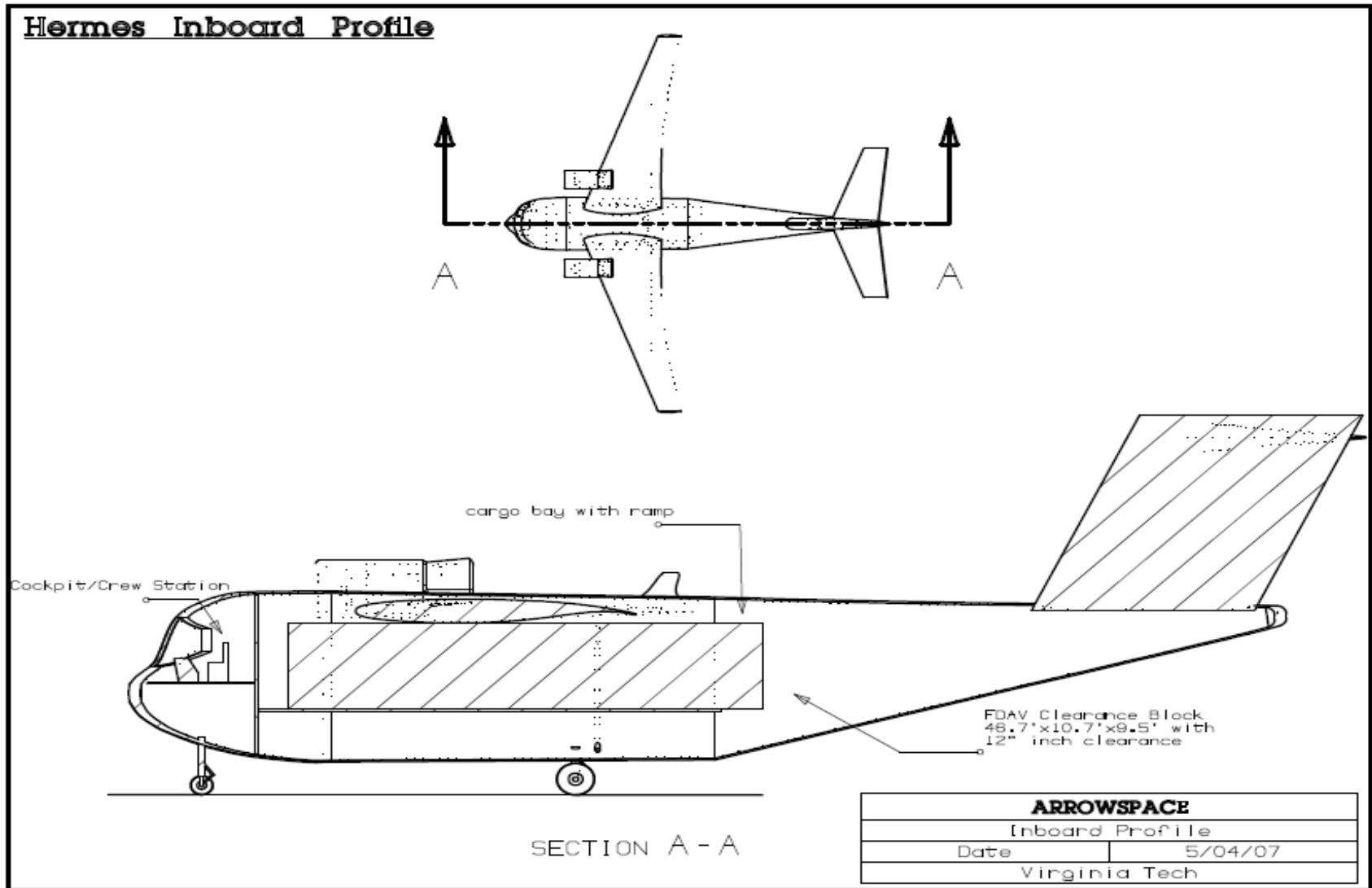


Figure 5-2: Hermes Inboard Profile

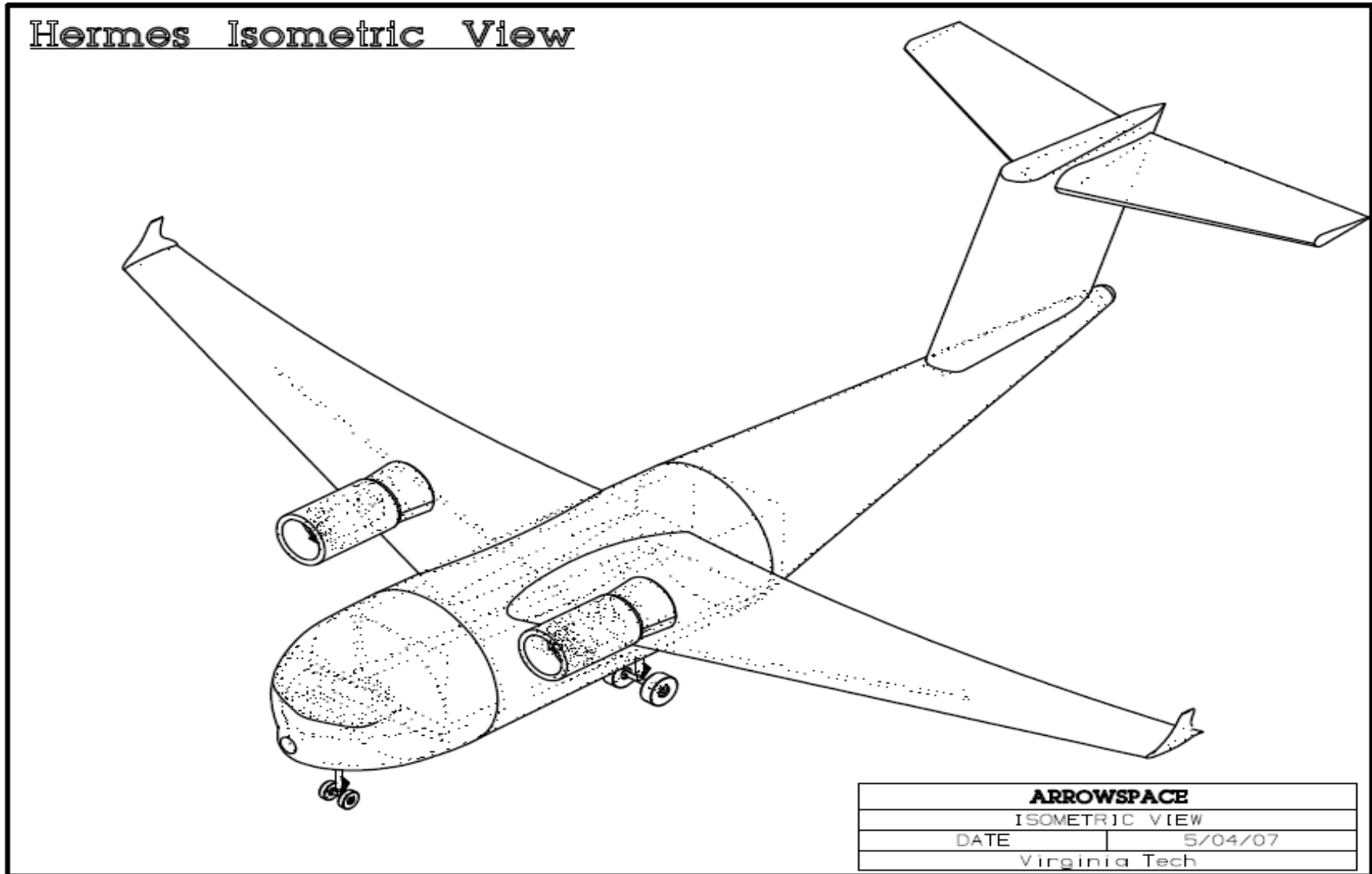


Figure 5-3: Hermes Isometric View

5.1 Fuselage

For some time, after the conceptual design phase, the fuselage design went mostly unchanged. However, once landing gear and systems considerations began to integrate into the design it became necessary to make drastic changes in the fuselage design. The lofting of the front part of the fuselage was reconfigured from a general bubble shape to stunted blunt nose in order to allow for the pilot and co-pilot to see more comfortably over the nose of the aircraft while still allowing enough space for systems (avionics, etc.). Likewise, the rear part of the fuselage was redesigned mainly because of landing gear requirements. It was found that if the geometry of the conventional design was used, the optimal placement of the landing gear would introduce an extremely small tail-scrape angle which would lead to tip-back angle problems. As a result, the diameter of the aft part of the fuselage was reduced to allow for the aircraft to achieve a safe landing.

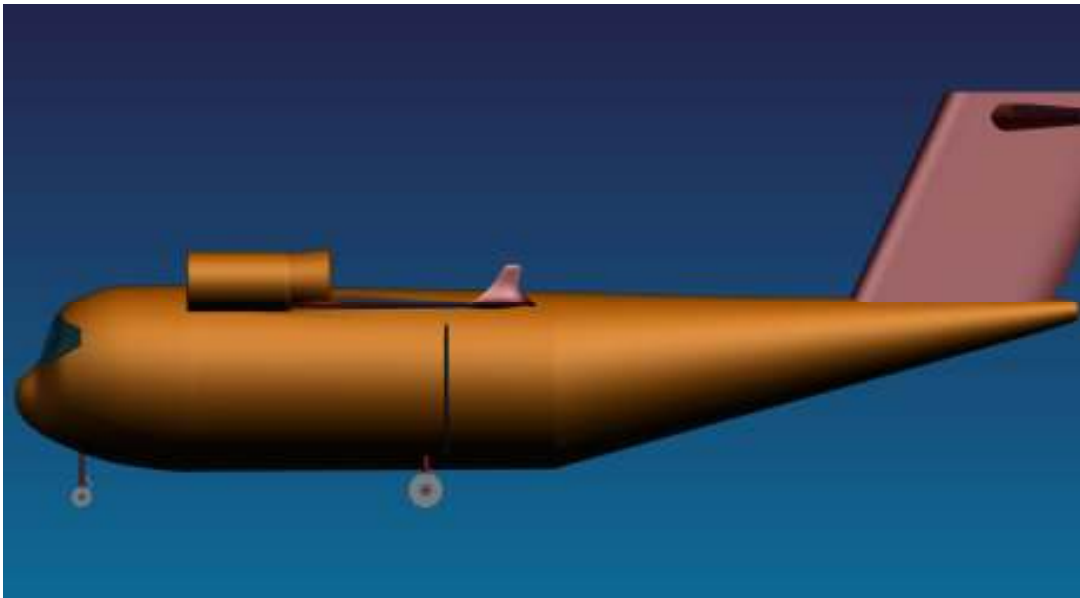


Figure 5-4: Hermes Fuselage

5.2 Wings and Engines

During the conceptual design phase potential wing planforms were analyzed but particular wing chord profiles and wing placement were not assessed. Through the evolution of the design a supercritical wing chord profile was chosen for use on Hermes to achieve increased lift along with winglets blended onto the wing. The placement of our wings was then chosen to be slightly forward of the center of gravity of Hermes.

From the conceptual phase, the engines of the conventional design were determined to employ upper-surface blowing and the same is true for the engines of Hermes. Extensive analysis was consequently done to determine the placement of the engines on the wings to achieve the greatest increase to lift possible.

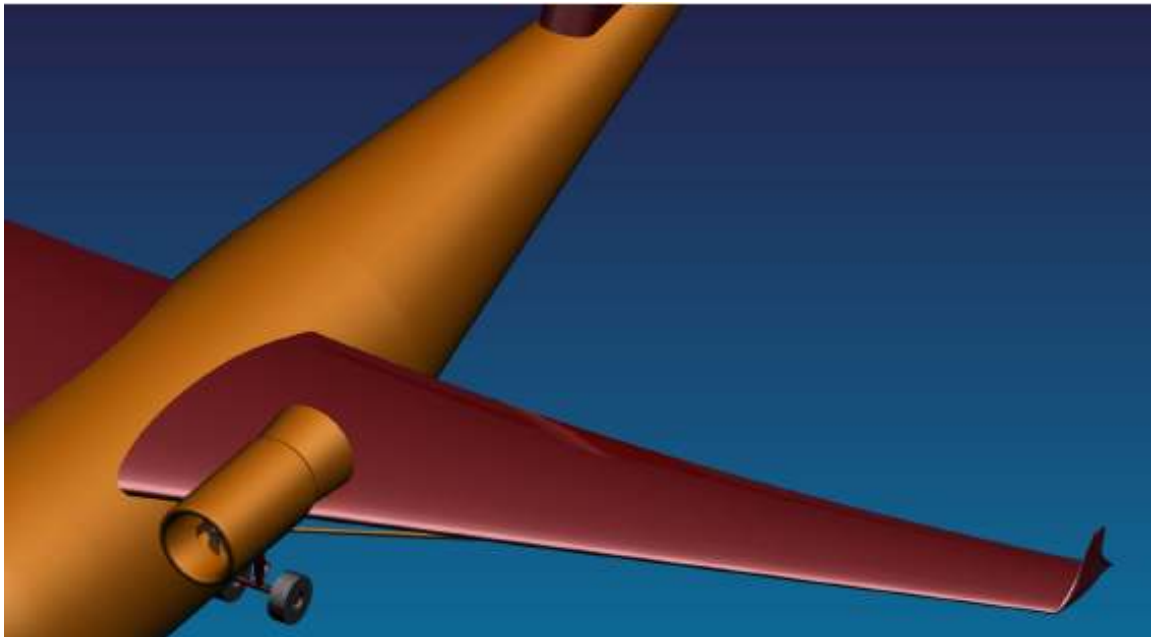


Figure 5-5: Close-up of Hermes Engine and Wing

5.3 Cargo Bay and Tail Assembly

The cargo bay area of Hermes was designed with enough space for the Future Deployable Armored Vehicle (FDAV) and its clearance requirement as stated in the Request for Proposal. Enough space in the cargo bay area has been set aside for additional systems and design features (stairs, seats, etc.).

As seen in figure 5-3 below, the horizontal and vertical tail combine to form a high T-tail design to aid in lifting Hermes.



Figure 5-6: Rear View of Hermes Cargo Bay and Tail Assembly

5.4 Cockpit

The cockpit design was not considered in the conceptual design phase but was fleshed out in the preliminary design phase to consider the flight crew's comfort and safety. Hermes cockpit design provides enough space for up to four people to work with efficiency and comfort. For safety concerns, the viewing angles for the pilot and co-pilot have been designed to conform to military specifications where the pilot must be able to see 15 degrees below a line parallel to normal line of sight.

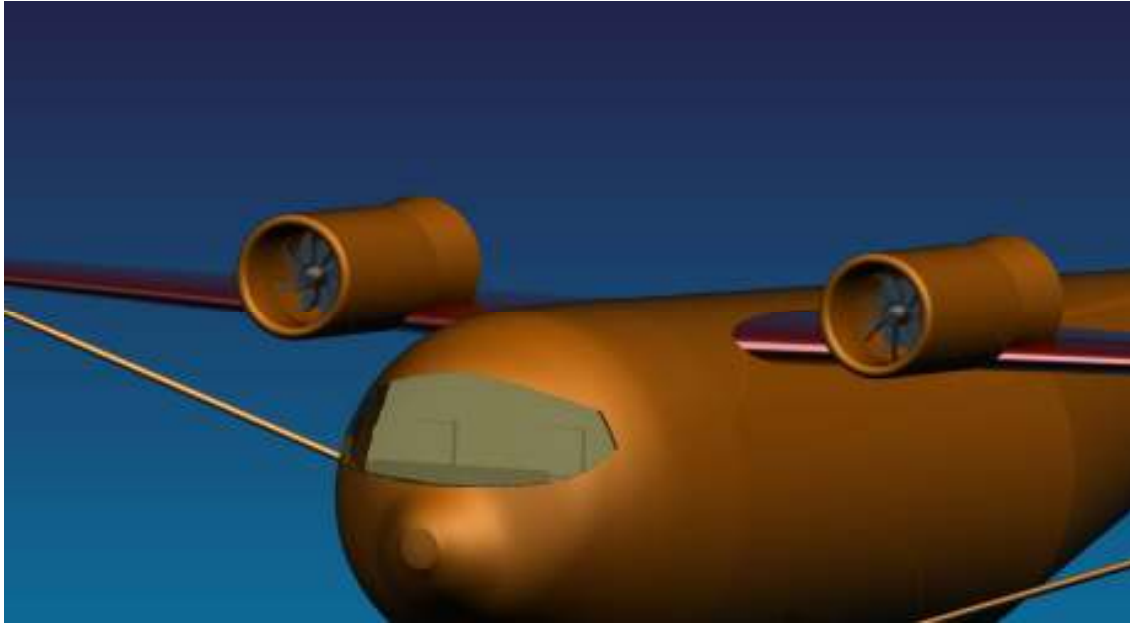


Figure 5-7: Close-up View of Hermes Cockpit

5.5 Landing Gear

Hermes makes use of a tricycle landing gear configuration. The sizing and placement of the landing gear have been analyzed with respect to the size and weight requirements of Hermes. As a result, the landing gear can support the aircraft in all conditions of operation and tip-back concerns are non-existent.

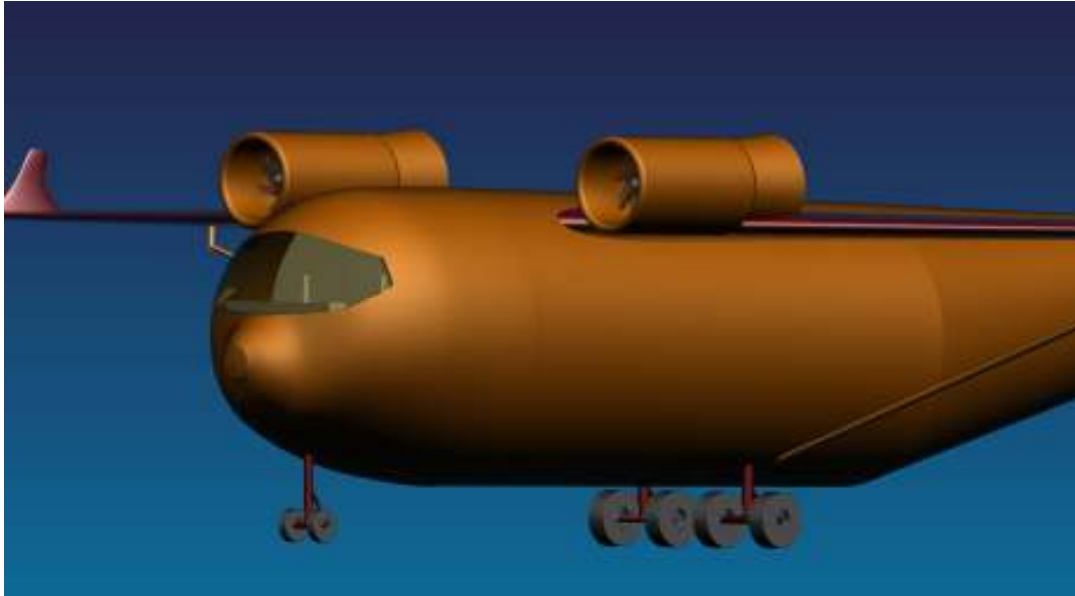


Figure 5-8: Close-up View of Hermes Landing Gear

5.6 Upper Surface Blowing

Hermes makes use of Upper Surface Blowing (USB) for powered lift to achieve the RFP requirements of short takeoff and landing. Upper Surface Blowing is a concept that takes advantage of the Coanda effect to increase the lift produced by an aircraft, usually during takeoff. In this configuration engines are mounted slightly above and forward of the wing in such a way that the engine exhaust can be vectored over the upper surface of the wing. During takeoff and landing an exhaust nozzle is used both to spread the flow and to direct it slightly downward over the wing surface. The vectored exhaust increases circulation and keeps the flow attached to the surface of the wing thus providing additional lift. Vortex generators can also be used to mix and energize the flow near the USB flap, located at the trailing edge of the wing directly behind the engine. During cruise, exhaust is not vectored so as to prevent interference with aerodynamic flow over the wing. USB systems have been proven on a number of aircraft including the YC-14, modified versions of the deHavilland DHC-5 Buffalo, and the Antonov AN-72. These aircraft all have STOL capabilities and such systems have been proven to greatly increase C_L during takeoff. Possible downsides to implementing a USB system include an increase in drag during cruise due to wing over-blowing which leads to higher fuel consumption rates.

6 Weight and CG Analysis

6.1 Component Weights

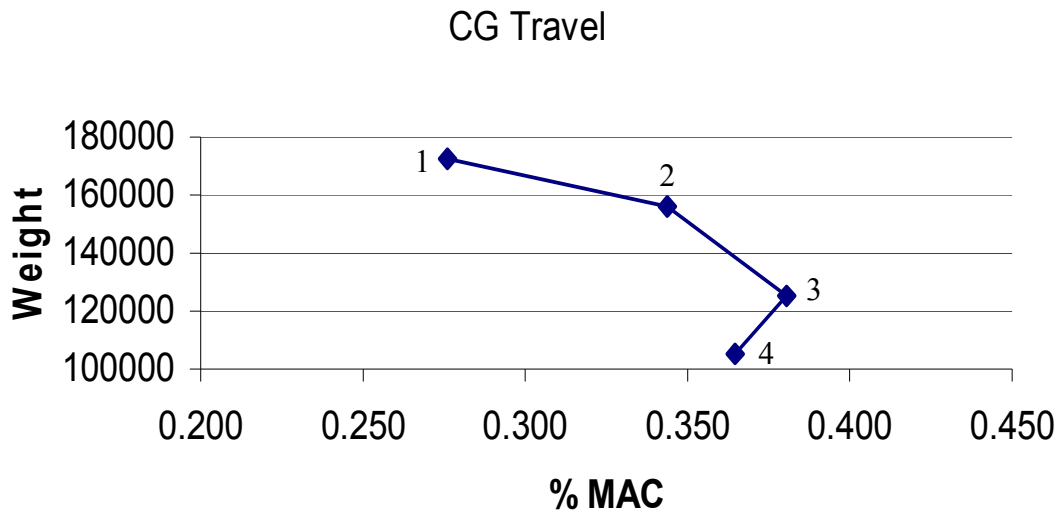
Aircraft component weights are particularly important in evaluating a design. Raymer's Aircraft Conceptual Design (ref. 34) method and Roskam's Aircraft Design (ref. 38) methods are used for calculating aircraft weights and center of gravity. The weight statements for the two missions with their respective center of gravity can be found in table 6-1. While most of the weights were estimated using the mentioned methods, a few weights were stated in the RFP such as crew and payload weights. Payload accounts for the difference in center of gravity between the primary and secondary missions. The fuel weight can change because the fuel tanks can carry more than needed for the primary mission. This analysis held fuel weight constant at the amount of fuel needed for the primary mission plus 10,875 lbs of fuel or twenty-five percent reserves. Fuel details will be discussed later.

Table 6-1: Weights and CG for Primary and Secondary Missions

COMPONENT	PRIMARY Weight (lbs)		SECONDARY Weight (lbs)	
	Takeoff	Landing	Takeoff	Landing
STRUCTURES				
WING	17014.9	17014.9	17014.9	17014.9
TAIL	9199.3	9199.3	9199.3	9199.3
BODY	15172.4	15172.4	15172.4	15172.4
LANDING GEAR	16570.5	16570.5	16570.5	16570.5
PROPULSION				
ENGINE INSTALLATION	7065.0	7065.0	7065.0	7065.0
ENGINE CONTROLS	15.0	15.0	15.0	15.0
STARTING SYSTEM	514.0	514.0	514.0	514.0
FUEL SYSTEM				
FUEL TANKS & LINES	266.3	266.3	266.3	266.3
INFLIGHT REFUEL SYSTEM	350.0	350.0	350.0	350.0
CONTROLS				
FLIGHT CONTROLS	3430.3	3430.3	3430.3	3430.3
FIXED EQUIPMENT				
INSTRUMENTS	268.3	268.3	268.3	268.3
HYDRAULIC AND PNEUMATIC	354.6	354.6	354.6	354.6
ELECTRICAL	944.9	944.9	944.9	944.9
AVIONICS	1538.3	1538.3	1538.3	1538.3
COUNTERMEASURES	500.0	500.0	500.0	500.0
FURNISHINGS AND EQUIPMENT	1700.0	1700.0	1700.0	1700.0
ANTI-ICE GROUP	550.0	550.0	550.0	550.0
PAYLOAD				
FLIGHT CREW	400.0	400.0	400.0	400.0
PAYLOAD CREW	200.0	200.0	200.0	200.0
CARGO	60000.0	60000.0	22046.0	22046.0
FUEL UNUSABLE	20.0	20.0	20.0	20.0
FUEL USABLE	43500.0	10875.0	43500.0	10875.0
CG (ft)	41.6	43.6	40.8	43.5

6.2 Center of Gravity

The center of gravity changes with the addition of payload and fuel usage. The CG shift due to fuel consumption is minimal because Hermes fuel tanks are located in the wings with no forward or aft tanks. Fuel pumps with computer assistance are used to distribute the fuel to the proper location for small weight shifts.



STATION	FLIGHT PHASE
1	TOGW
2	CRUISE
3	LANDING
4	CARGO DROP

Figure 6-1: Center of Gravity Travel for Different Phases

7 Aerodynamics

This airplane is aerodynamically designed to be an inter-theater tactical transport with austere STOL capability. Therefore, it is essential for this design to have the potential for high lift and the ability for an extensive range. The RFP calls for a takeoff distance which does not exceed 2,500 ft and a landing distance between 2,000 ft and 3,000 ft. Additionally, the design must endure a range of 3,200 n miles for the Ferry mission.

7.1 Wing Planform

From the initial sizing constraints, a wing loading of approximately 70 psf was determined. Using this wing loading and the initial weight fractions, the preliminary planform area was estimated to be 2500 ft².

Further analysis began after estimating a reasonable value for wing area. The design requirements call for a STOL aircraft which suggests using a high aspect ratio wing contributing to more lift at take off. Additionally, a higher aspect ratio will allow for better cruise efficiency so that a range of 3,200 nm can be more easily attained. Driving the aspect ratio higher implies a larger span which requires a stronger load bearing member at the wing root. For larger wing spans, it was determined that struts be implemented into the design to relieve the root bending moment and effectively increase the thickness. (ref. 24) This means a thinner, and hence more transonically efficient, airfoil could be used while still allowing ample room for fuel. After several iterations and design changes the initial wing span was extended. Various planforms were considered and subsequently altered to best meet our requirements. These planforms are shown in figure 7-1.

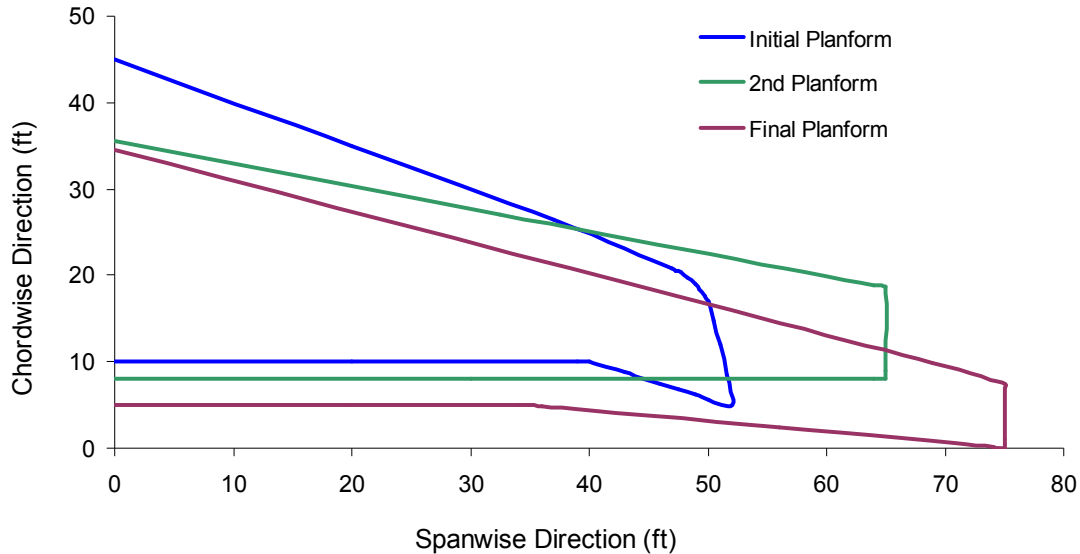


Figure 7-1: Planform Geometries

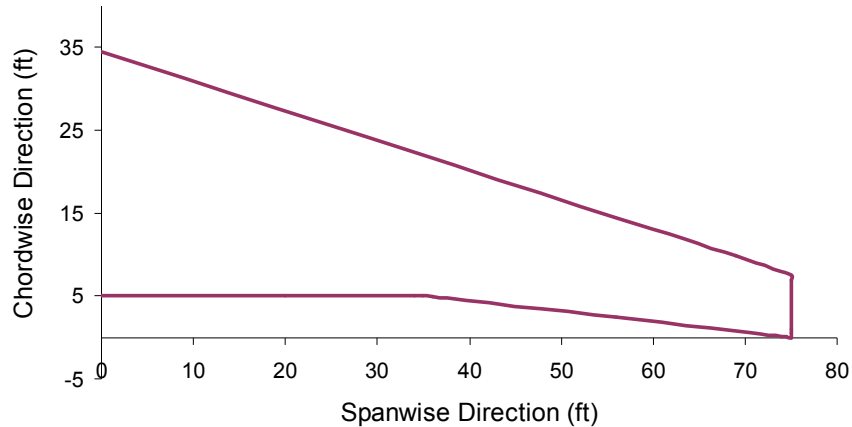
The initial wing planform was designed with low sweep and a total wing span of about 110 ft. After this sketch was made, it was analyzed using a program called Wing Planform Analysis. (ref.27) From this program, leading and trailing edge locations on the wing were inputted and resulting aerodynamic parameters were outputted. The parameters outputted in the Wing Planform Analysis Program include: planform area, mean aerodynamic chord, x-centroid, spanwise position of MAC, x-leading edge of MAC, quarter chord of MAC, aspect ratio, average chord, and taper ratio.

Shortly after creating this initial planform, it was decided that a longer span was needed to increase the wing's aspect ratio; thus the 2nd planform was created. To modify a planform, the area was kept unchanged, while the root and tip chords and the span were changed. Thus, when the 2nd planform was created, it had the same required constraints as the initial planform as well as the preferred wing span.

The final planform was designed so that the wing would have a larger inboard area. This was necessary due to USB on the wings. In the USB configuration, the engines are mounted on the inboard portion of the wings. The larger inboard area was added so that there is more area aft of the USB configuration, aiding the high lift system. There was a resulting extra sweep at the trailing edge of the wing tip so that an area of 2500 ft² could be maintained. The span was also lengthened so that the area could be maintained. The figure showing the final wing planform can be seen in figure 7-2, along with relevant dimensions shown in table 7-1.

Table 7-1: Planform Parameters

Reference Area (ft ²)	2527
Half Span (ft)	75
Average Chord Sweep (degrees)	20
Aspect Ratio	8.9
Mean Aerodynamic Chord (ft)	19.1

**Figure 7-2: Wing Planform**

7.2 Airfoil Selection

The first step in choosing an airfoil was to study other tactical transport vehicles and the aerodynamic configurations they used. It was found that most of these vehicles fly in transonic flight conditions much like what is required for Hermes. Among these vehicles found, it was remarked that supercritical airfoils were the most prevalent. Supercritical airfoils have a larger leading edge radius than subsonic airfoils. This helps with controlling the expansion around the upper surface which serves two purposes; subjecting the flow to a large pressure gradient while the boundary layer is thin and can sustain it, and to create higher lift at low speeds. Controlling the expansion and compression of the flow around the airfoil is significant in preventing separation and shock losses during cruise. Since supercritical airfoils function well in both subsonic and transonic speeds, the supercritical airfoil was the chosen type of airfoil because the design requires both transonic and low subsonic performance to achieve efficient cruise and STOL field performance.

Using the Korn Equation, it is easy to conclude that a supercritical airfoil with 10 to 14 percent thickness to chord ratio and with medium to high design lift be chosen. Minimizing thickness is paramount in delaying drag divergence. To select the appropriate supercritical airfoil, the program TSfoil2 (ref. 32)

was utilized. Several supercritical airfoils were run through the program using variable free stream mach numbers to analyze the airfoil's behavior at different flight regimes. The airfoils used in TSfoil are listed in the table below.

Table 7-2: Airfoils Tested in TSfoil

Airfoils	
SC(2)-0010	SC(2)-0710
SC(2)-0012	SC(2)-0712
SC(2)-0410	SC(2)-0714
SC(2)-0412	SC(2)-1010
SC(2)-0414	75-07-15
SC(2)-0610	82-06-09
SC(2)-0612	70-10-13
SC(2)-0614	71-08-14

Using our selected planform sweep, the effective thicknesses and perpendicular Mach numbers for the airfoils were accounted for in the test runs. In each run, the pressure distributions were plotted so that the lift across the airfoil could be analyzed. The best three pressure distributions out of all the airfoils tested are plotted below.

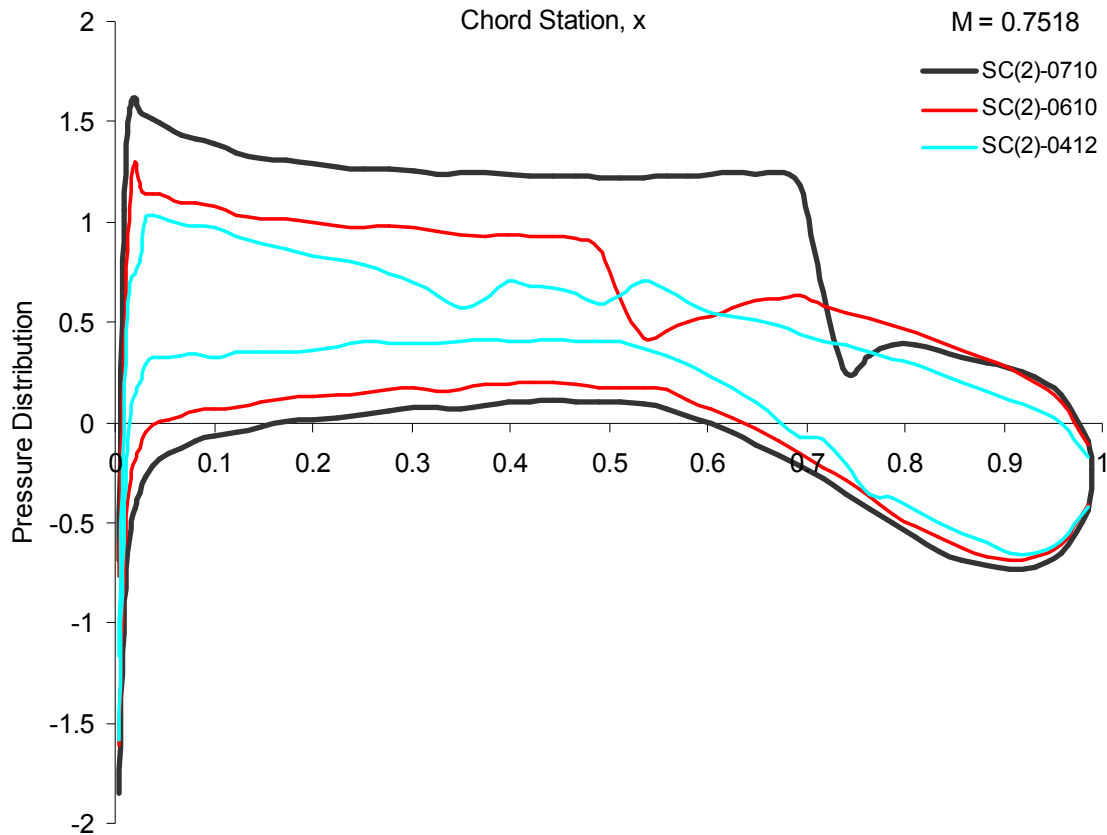


Figure 7-3: Pressure Distribution for SC(2)-0412, SC(2)-0610, SC(2)-0710

After thorough analysis of the pressure distributions, the SC(2)-0710 airfoil was chosen to be the most suitable for Hermes. From the above pressure distributions it can be seen that there is a slightly greater aft loading for the SC(2)-0710 airfoil and the shock is weak and farther aft along the chord than the other two airfoil's shock. Also there is a larger pressure gradient for the SC(2)-0710 showing that there is more lift for this particular airfoil. Figure 7-4 shows the geometry of the SC(2)-0710 airfoil.



Figure 7-4: The SC(2)-0710 Airfoil

For this series of airfoil, the 07 indicates the design lift coefficient in tenths and the last two digits indicate the airfoil's maximum thickness to chord ratio in hundredths. The design lift coefficient for the SC(2)-0710 airfoil proved to be fitting because it fell within the desired range for design lift. An airfoil

with 10 percent thickness to chord ratio was selected because it produced the desired results for the required cruise mach when running the TSfoil program. The program was run using the established wing sweep of 20 degrees and the combination of this wing sweep and this t/c ratio gave the best results. If the t/c ratio was to be any higher than 10 percent t/c, then the wing sweep would need to be increased, thus increasing the associated structural weight.

Section lift curve data was found using the TSfoil program. The program was run for cruise conditions with a perpendicular Mach number of 0.7518, corresponding to a free stream Mach number of just above 0.80. The plot for the section lift curve is shown below in Figure 7-5.

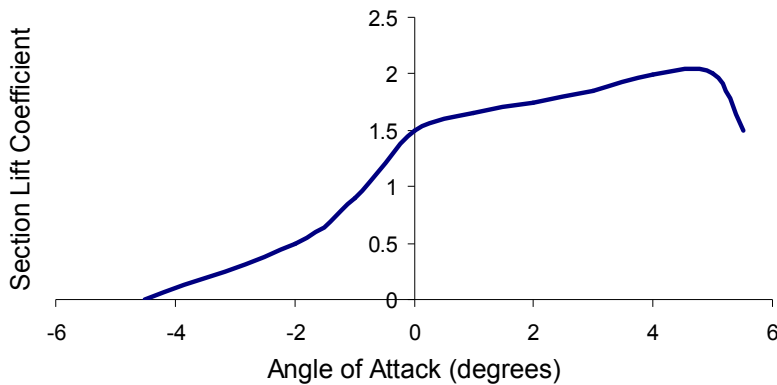


Figure 7-5: Section Lift Curve Slope

Additionally, the pressure distribution for the SC(2)-0710 airfoil was found using the program TSfoil. The program was run using cruise conditions and zero angle of attack. The plot for pressure distribution is presented in Figure 7-6.

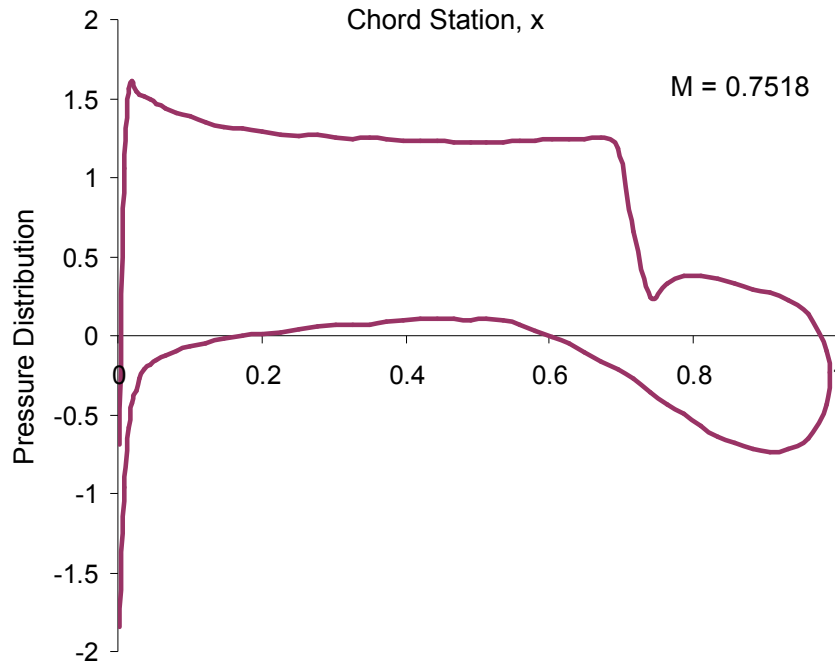


Figure 7-6: Pressure Distribution at Cruise Conditions

Symmetric airfoils were chosen for the horizontal and vertical tails. The horizontal tail is a NACA 0012 airfoil and the vertical tail is a NACA 0013 airfoil. The airfoil selections are discussed more in the Stability and Control section.

7.3 Wing Analysis

The location of the wings on the fuselage was estimated using a method found in Raymer. (ref. 34) This method used the CG location and the wing's MAC to determine the specific location. The figure below demonstrates the location of the root chord on the fuselage.

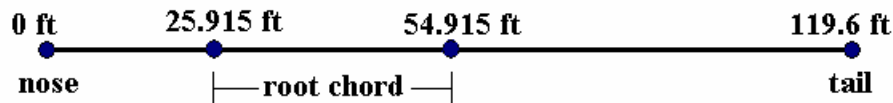


Figure 7-7: Location of Wing on Fuselage

Using design software, the lift coefficients for takeoff, landing and cruise were analyzed. As it was mentioned earlier, the program TSfoil was utilized to estimate the lift coefficient at transonic speeds or cruise. Similarly, the program Xfoil was used to estimate the lift coefficient at subsonic speeds, or takeoff

and landing. The figure below demonstrates the difference in lift coefficient for varying angles of attack at takeoff, landing and cruise.

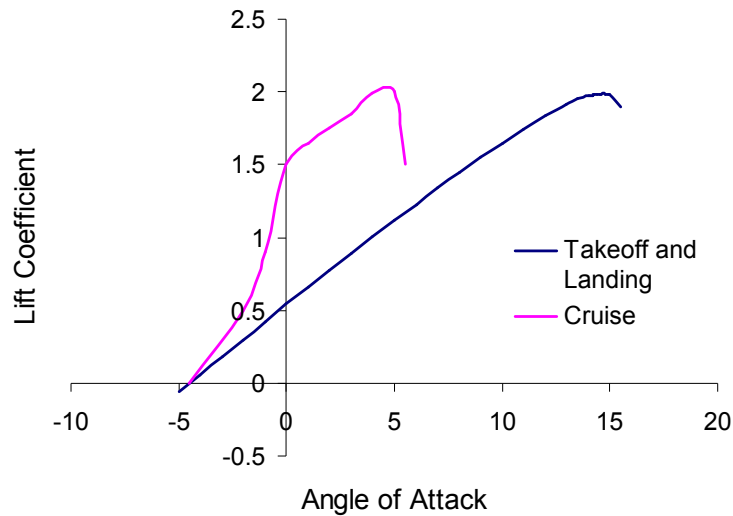


Figure 7-8: Lift Coefficient for Takeoff, Landing and Cruise

7.4 High Lift Selection

The design requirements call for a takeoff distance of no more than 2,500 ft and a landing distance between 2,000 ft and 3,000 ft which suggests the need for high lift devices. In examining other STOL transport vehicles, it was decided that an Upper Surface Blowing (USB) system be used as the primary high lift device. The configuration for a USB system consists of mounting the engines forward and above the wing. As a result of the Coandă effect, air flow from the engines stays attached along the wing and flaps and is then deflected downwards to create lift. This system will result in shorter takeoff and landing distances, ideal for the STOL requirement (ref. 16).

To land in such a short distance, there needs to be plenty of drag present during landing. Therefore, fowler flaps were implemented into the design. Fowler flaps operate by extending away from the wing and then hinging downwards thus creating more area on the wing. The increased area will help increase drag during landing so that the aircraft can slow down more rapidly (ref.3).

Furthermore, there will be Krueger flaps running along the inboard portion of the wing's leading edge and slats running along the outboard portion of the wing's leading edge. When the Krueger flaps are

unhinged and the slats deployed, the aircraft will fly at slower speeds. This will aid in takeoff and landing so that the aircraft can fly slower and, therefore, takeoff and land in shorter distances (ref.12).

Because the aircraft will be operating at low speeds during takeoff and landing, vortex generators will be added to the upper surface of the wing. Vortex generators are necessary because at low speeds close to the ground, the air circulates around the wing resulting in flow separation near the flap. To prevent this from happening, vortex generators will be present at takeoff and will retract when the flaps are raised (ref.42).

Some additional features on the wings were winglets and struts. Winglets were incorporated into the wings to lower drag while keeping good wingtip flow. Struts were implemented to allow a thinner wing with a higher aspect ratio, but without the weight penalty.

With the aid of the high lift system and aerodynamic surfaces, the effect on lift is greatly altered. Using the program XFOIL (ref.4), it was found that at takeoff, the most section lift the SC(2)-0710 airfoil will give is only about 2 at a 15 degree angle of attack. However, when the high lift device and aerodynamic surfaces are introduced, the lift increases much more. Estimations of the maximum increase of lift with the use of flaps, slats, and USB are shown in Figure 7-9. These estimations were based on wind tunnel tests from a comparable aircraft with USB in Figure 15 of the AIAA-1975-868 paper (Ref.16).

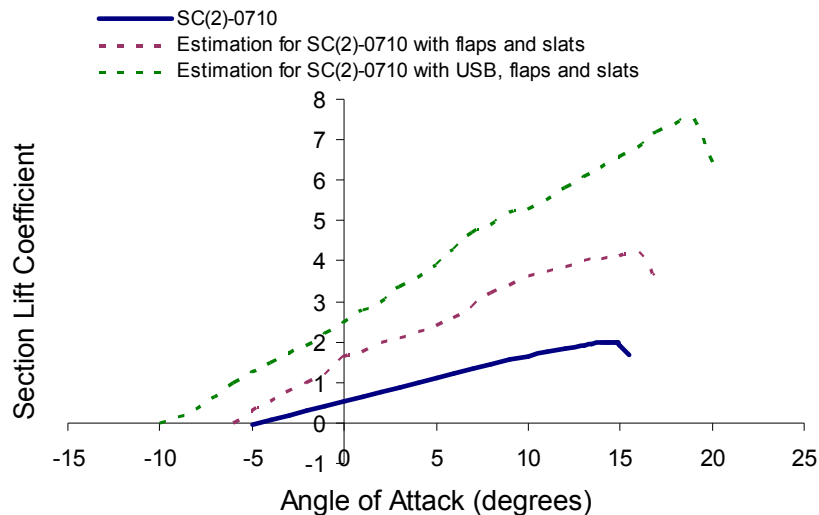


Figure 7-9: Section Lift Curves with High Lift

7.4.1 Spanload Distribution

Planform analysis in VLMpc and AVL both revealed that Hermes' planform does not lift elliptically; the ideal scenario. Given the planform geometry of Hermes as input, an optimizing code, LamDes (ref. 19), was used to compute a wing twist that would provide an elliptic spanload and hence minimize drag. However, these twist distributions often are hard to manufacture and tricky to integrate. In lieu of this, wing twist was altered using a method known as the straight line wrap method (ref. 23).

LamDes minimizes the sum of the pressure and induced drags while the straight line wrap provides a more general, simple approach to wing twist. From an aerodynamics perspective the LamDes solution makes more sense because of the associated efficiency achieved through the optimization algorithm. From a manufacturing perspective, the straight line wrap would be more feasible; one reason being the smaller twist slopes between spanwise locations simplifies wing integration. The straight line wrap is only dependent on the root and tip twists, which were taken from the LamDes results for comparison. Figure 7-10 shows a comparison of the LamDes results with the straight line wrap method. To minimize manufacturing costs, the straight line wrap results were employed in the design. Using this method, it is shown that approximately 2 degrees of wing twist would be needed for Hermes.

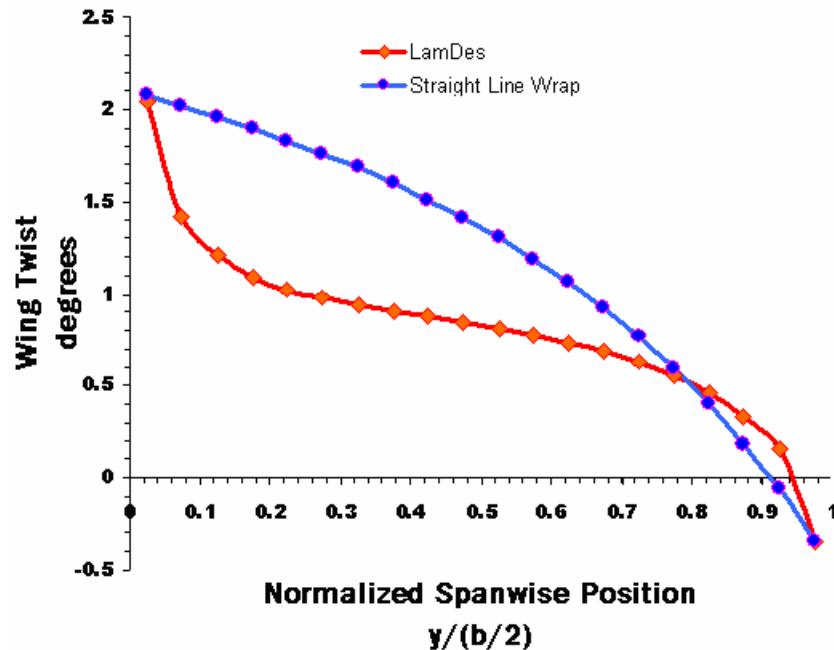


Figure 7-10: Hermes Wing Twist Selection

7.5 Drag

To determine drag for Hermes throughout different flight regimes, Raymer's (ref. 29) component drag buildup method was utilized. This method uses Reynolds number, the flat-plate skin friction coefficient, form and interference factors, and wetted areas to calculate the parasite drag. The components making up the total parasite drag included wings, fuselage, canopy, nacelle, and tail.

From Raymer(ref. 34), it was also determined that the leakage and protuberance drag was to be 4% of the overall parasite drag. Additionally, the transonic drag rise was determined using Raymer's (ref. 34) graphical estimation, and wave drag was calculated using the Sears-Haack body wave drag equation from Raymer (ref. 34). Induced drag was also calculated using Raymer (ref. 34). For takeoff and landing, the effect of flaps and landing gear was applied to the drag estimations. These calculations were also made using Raymer (ref. 34).

7.5.1 Drag Breakdown

The buildup of drag at each flight regime is shown below in the drag buildup tables. In addition, the drag buildup at cruise is shown in Figure 7-11. The drag buildup includes all parasite drag, leakage and protuberance drag, and induced drag. These are all present in takeoff, cruise and landing. However, at takeoff and landing, the landing gear will additionally contribute to the total drag. Similarly, at landing, the flaps will contribute to the total drag. And at cruise, wave drag contributes to the total drag. All flap and landing gear drag calculations were made using Raymer (ref. 34).

Table 7-3: Zero-Lift Drag Buildup for Take Off

Component	ΔC_D	% Total
Wing	0.00888	27.2 %
Horizontal Tail	0.00188	5.8 %
Vertical Tail	0.00302	9.2 %
Fuselage	0.00817	25.0 %
Enclosure	0.00260	8.0 %
Appendages		17.4 %
Nacelle	0.00389	
Vortex Generators	0.00115	
Antennas	0.00038	
Pitot Tube	0.00004	
Angle of Attack Indicators	0.00004	
Anti-Collision Lights	0.00004	
Radar Altimeter	0.00015	
Landing Gear	0.00211	6.4 %
Micellaneous	0.00034	1.0 %
Total Zero Lift Drag Coefficient	0.03269	100 %

Table 7-4: Zero-Lift Drag Buildup for Cruise

Component	ΔC_D	% Total
Wing	0.00888	29.0 %
Horizontal Tail	0.00188	6.1 %
Vertical Tail	0.00302	9.9 %
Fuselage	0.00817	26.7 %
Enclosure	0.00260	8.5 %
Appendages		18.6 %
Nacelle	0.00389	
Vortex Generators	0.00115	
Antennas	0.00038	
Pitot Tube	0.00004	
Angle of Attack Indicators	0.00004	
Anti-Collision Lights	0.00004	
Radar Altimeter	0.00015	
Micellaneous	0.00034	1.1 %
Total Zero Lift Drag Coefficient	0.03058	100 %

Table 7-5: Zero-Lift Drag Buildup for Landing

Component	ΔC_D	% Total
Wing		63.3 %
Affected by Flaps	0.03219	
Not Affected by Flaps	0.00888	
Horizontal Tail	0.00188	2.9 %
Vertical Tail	0.00302	4.7 %
Fuselage	0.00817	12.6 %
Enclosure	0.00260	4.0 %
Appendages		8.8 %
Nacelle	0.00389	
Vortex Generators	0.00115	
Antennas	0.00038	
Pitot Tube	0.00004	
Angle of Attack Indicators	0.00004	
Anti-Collision Lights	0.00004	
Radar Altimeter	0.00015	
Landing Gear	0.00211	3.2 %
Micellaneous	0.00034	0.5 %
Total Zero Lift Drag Coefficient	0.064881	100 %

The total drag for the aircraft is made up of the total zero-lift drag, or parasite drag, the leakage and protuberance drag, induced drag, and wave drag. In the table below, the total drag is given from take-off, cruise and landing. The parasite drags in the table are the values for the zero lift drag at take-off, cruise, and landing calculated previously.

Table 7-6: Total Drag Buildup

	Parasite	Leakage and Protuberance	Induced	Wave	Total C_D
Take-Off	0.03269	0.00131	0.091	--	0.1250
Cruise	0.03058	0.00122	0.010	0.003	0.0448
Landing	0.06488	0.00259	0.155	--	0.2225

The following plot also shows the buildup of the total drag. The plot includes parasite, leakage and protuberance, induced and wave drag. In the plot the parasite drag is broken up into its individual components. Instead of displaying the total parasite drag, the plot shows the fuselage drag, wing drag, tail drag, canopy drag, and nacelle drag combined as the parasite drag. The combination of parasite drag is displayed as blues and purples while the induced and wave drags are red and pink. Also the drag divergence Mach number of 0.76 is shown in the figure.

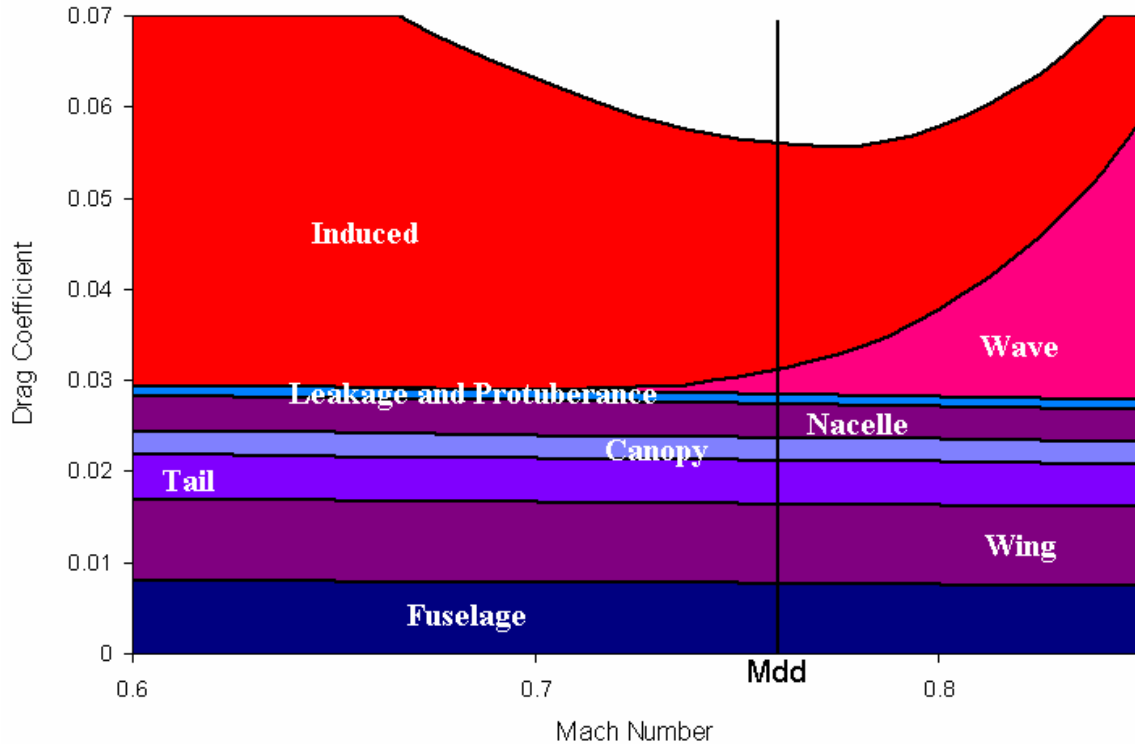


Figure 7-11: Drag Buildup at Cruise

7.5.2 Drag Polar

In the three figures below, the drag polars for takeoff, cruise, and landing are shown. The drag polar for take off was calculated for angles of attack between 0° and 15° . The drag polar for landing was calculated for angles of attack between -10° and 15° , and the drag polar for cruise was calculated for angles of attack between -5° and 5° . These drag polars show 0 and 100% suction as well as the trimmed drag polars. Additionally, the design lift coefficient is shown in each of the plots. All calculations were made using Mason (ref. 21).

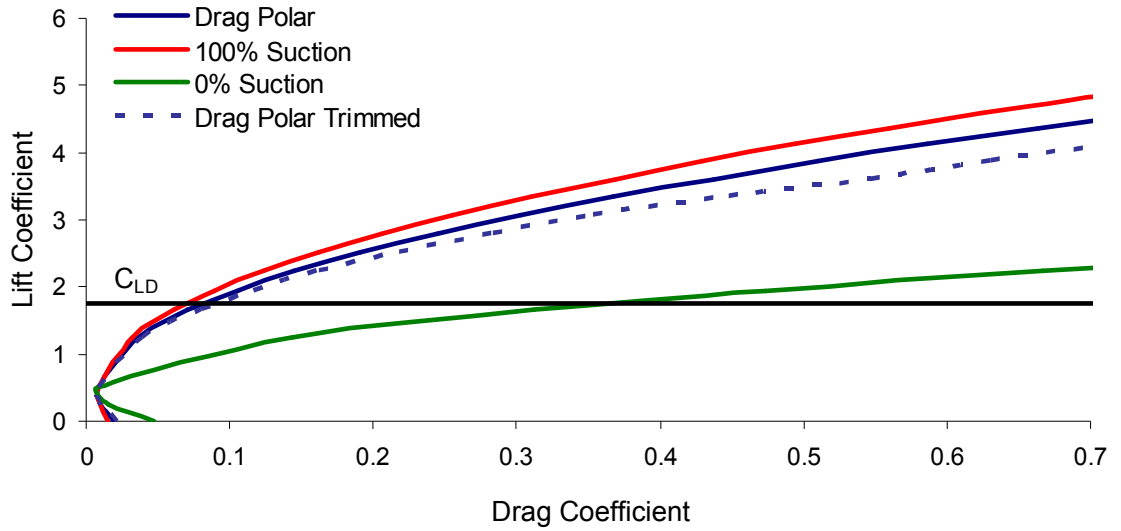


Figure 7-12: Drag Polar for Take Off

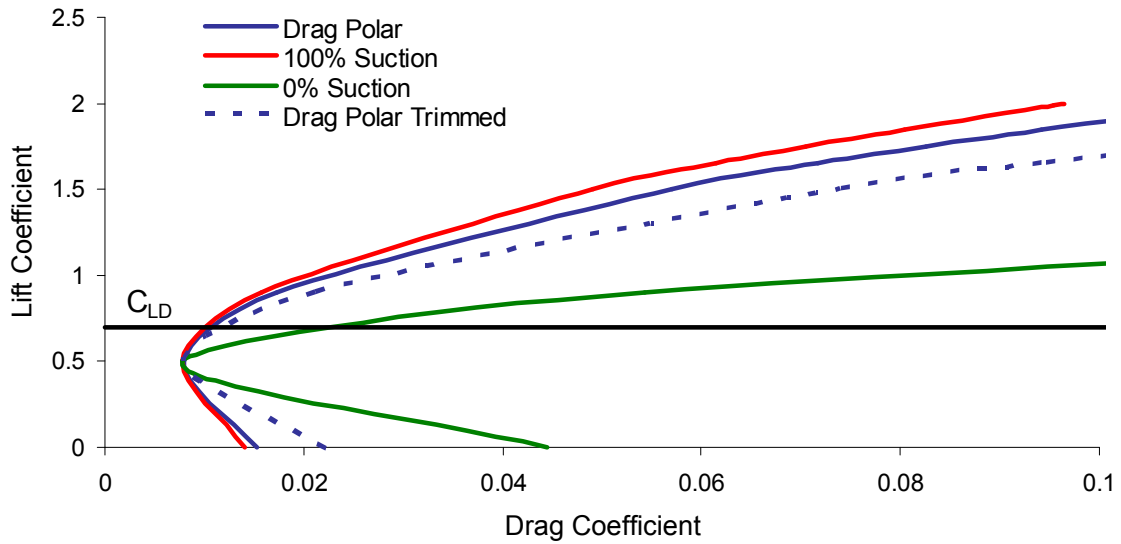


Figure 7-13: Drag Polar for Cruise

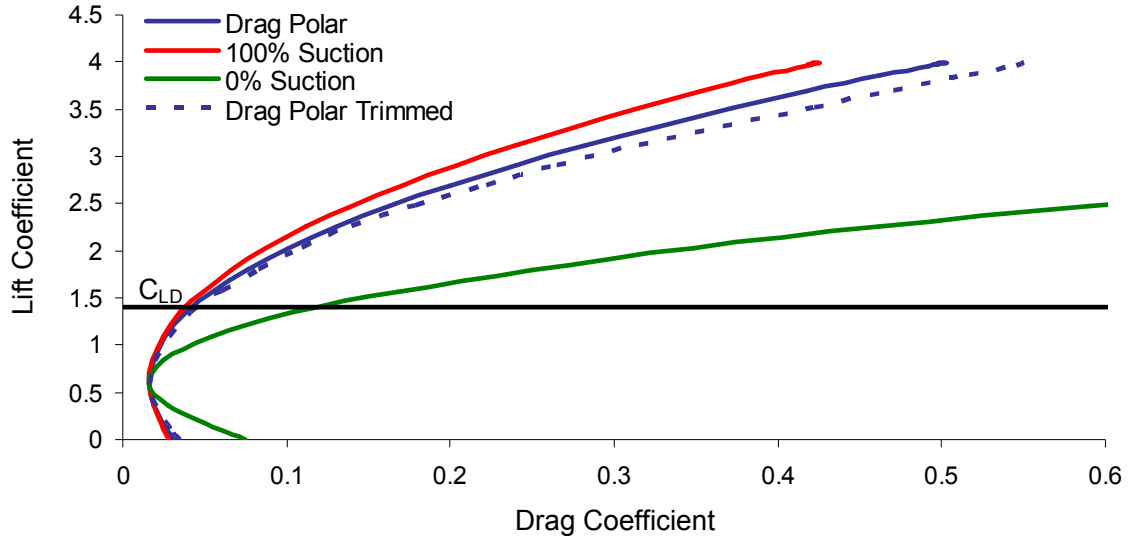


Figure 7-14: Drag Polar for Landing

From the drag polar plots above it can be seen that the drag polars for takeoff, cruise, and landing are all very efficient. The drag polar for takeoff and landing incorporate the effect of the USB into the lift, thus the values of lift are increased by a factor of approximately 3.0.

8 Propulsion

Due to the specific RFP requirements of short takeoff and landing, the design of the propulsion system for Hermes was of particular importance. Considerations for the selection of a propulsion system included meeting the performance requirements, reliability, cost, maintainability, and safety.

8.1 Engine Configuration and Selection

The three initial design concepts demonstrated a wide range of possible engine configurations utilizing two, three, or four engines. Therefore, one of the first propulsion considerations was to determine how many engines were appropriate for the given application. It was found that for the given situation and configuration, a twin engine aircraft would have several benefits over a three or four engine design. A twin-engine aircraft is less complicated mechanically and allows for fewer moving parts which in turn leads to less overall maintenance and cost. Using Roskam's sizing methods (ref. 42) along with the AIAA engine deck it was also confirmed that an increase in engine number leads to an overall increase in weight and drag for the aircraft.

Because of federal and military regulations on engine-out flight as well as the performance criteria, however, the propulsion system on a twin-engine aircraft has the potential to become significantly oversized. Engine-out requirements ensure that the engines are large enough for the aircraft to remain operational in the case of a mechanical failure. This also means a slight increase in TOGW for the twin-engine configuration, but allows for the possibility of takeoffs much shorter than the RFP requirement and increased in-flight maneuverability when all engines are operating at full power. It is understood that a twin-engine design will perform comparable to a four-engine design in AEO flight; however a critical engine inoperative (CEI) scenario imparts uneven moments on the aircraft and the loss of all USB capabilities on the side of the engine failure. One possible way of limiting the moment and regaining the USB performance is by mechanically cross linking the engines (ref. 35). This allows the operating engine core to run the fans on both engines and regain some moment symmetry and USB performance and the side of the failure. Based on these considerations, a cross-linked, twin-engine design was chosen for Hermes.

Next, it was necessary to decide between high or low bypass turbofan engines. All three designs concepts incorporated an engine with a high bypass ratio due to the need to maximize static thrust at takeoff. A high bypass engine produces more thrust per fuel consumption at low speeds and altitudes yet is still efficient in cruise around Mach .8, so this is the ideal choice for a STOL transport (ref. 16).

Finally, the engines had to be sized for the aircraft. In analyzing the AIAA engine deck, Raymer's method for calculating installation losses was used (ref. 34). It was found that the engine deck could only be reasonably sized for a twin-engine configuration given the installation adjustment of about 2.7% and the constraints of .4 on T/W and 182,820 lbs on TOGW. Since the performance requirements corresponded to the most maintainable and cost-effective solution, the AIAA engine deck was chosen as an acceptable engine model. To check the AIAA engine deck against existing production turbofans, GE engines were researched. It was found that performance was similar and that a CF-34 series engine could be applied to a four engine Hermes or a CF-6 series to the preferred twin-engine layout (ref. 5).

Upon further analyzing the performance characteristics of the AIAA engine, presented in figure 8-1, it was found that this engine produces sufficient thrust at an acceptable fuel consumption and can be scaled within range to meet the performance requirements quite well. When sized to the design constraints of .4 thrust to weight ratio and 182,820 lbs TOGW, each engine was found to be a modest 7065 lbs and 120" in length by 70" in diameter. Therefore, in the preferred design concept, two AIAA engines with a bypass ratio of 6 and scaled down to 88.5% were chosen. The final engine sizing based on the selection criteria is presented in table 8-1.

Table 8-1: Engine Sizing

Performance	
Required T/W	.4
Required TOGW (lb)	182,820
Required Thrust (lb)	73,100
per engine (lb)	36,550
Scale Factor	88.5%
Scaled Flow (lb/sec)	1178
Dimensions	
Weight per engine (lb)	7065
Length of engine (in)	120
Diameter of engine (in)	77
Nacelle Length (in)	235
Inlet Diameter (in)	85

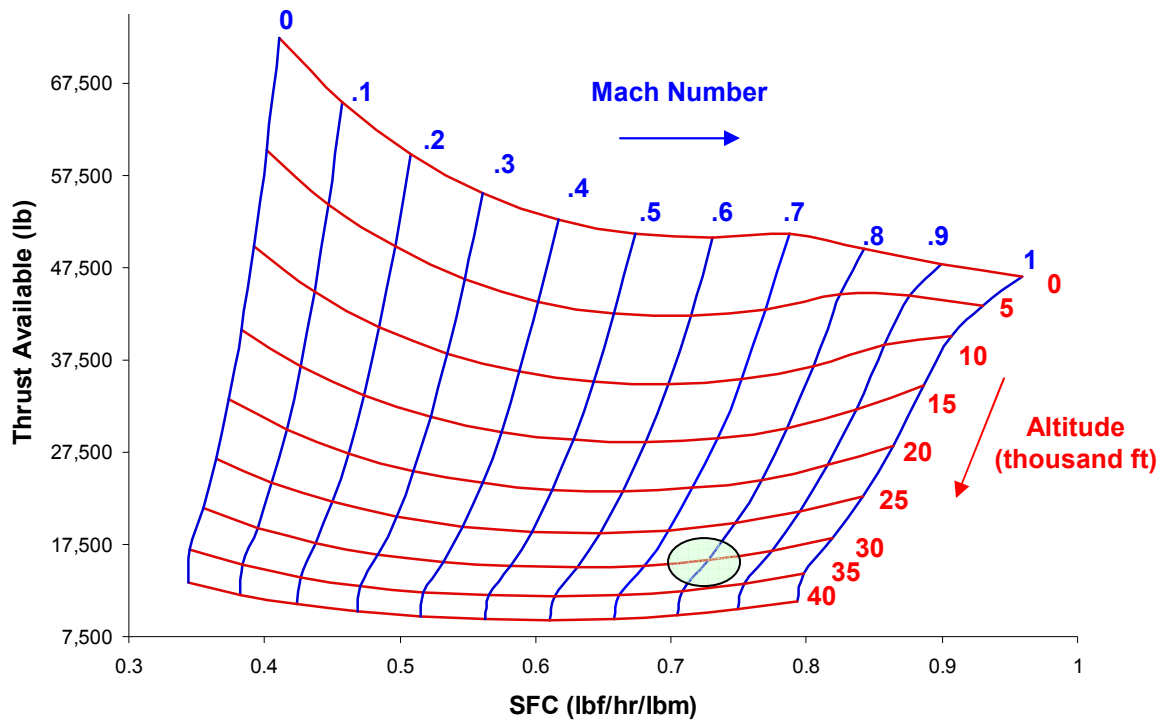


Figure 8-1: Engine Map for a Pair of AIAA Engines at Full Power

8.2 Inlet and Nacelle Sizing

Using the sizing method described in Roskam (ref. 42), the necessary inlet diameter was calculated to be a little over 10% larger than the engine diameter for the given aircraft sizing, or 85 inches. A fixed geometry inlet of this size allows enough airflow to match the performance criteria needed for takeoff, prevents shocks, and remains efficient in cruise.

For a design cruise Mach number of .8, a subsonic podded nacelle is used to control the flow into and around the engine and prevent the blade tips of the first stage compressor from reaching supersonic speeds. The inlets are located far enough away from the fuselage and forward of the leading edge of the wing to minimize the disturbance of the flow entering the engine. As pictured in figure 8-1, a long-ducted nacelle encloses the entire engine and is used to direct both the fan and engine exhaust over the surface of the wing from a common nozzle (ref. 16). In the Hermes's USB configuration, the over-wing podded nacelles will help reduce ingestion of debris on unprepared runways and, as found by the Quiet Short-Haul Research Aircraft Flight Research Program, will also lower the overall noise footprint produced by the propulsion system (ref. 7).

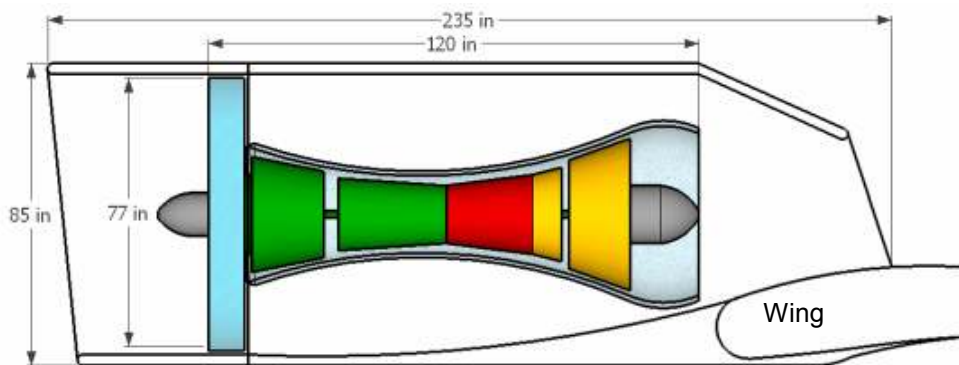


Figure 8-2: Cutaway View of Engine and Nacelle Layout

8.3 Exit Nozzle

After considering variable geometry nozzles, spread nozzles, and D-nozzles, a D-nozzle with side flaps, similar to that on the YC-14 (ref. 9), was chosen for Hermes. This nozzle was found to be relatively

simple, very effective, and well-documented and was thus the optimum choice. A D-nozzle does not significantly affect the stability and control or aerodynamic characteristics of the plane in the same way that a spread nozzle does, or is it as mechanically complicated as most variable geometry nozzles (ref. 6). By employing side flaps, a nozzle with a physical aspect ratio between 3 and 4 can obtain an effective aspect ratio over two times that. This puts the USB performance on par with spread nozzles of $AR = 7-10$ that Boeing found to be optimally sized for NASA (ref.6). Therefore, Hermes makes use of a 3.5 aspect ratio D-nozzle with an inboard flap capable of a 15° deflection and an outboard flap capable of a 30° deflection, as seen in figures 8-3 and 8-4. These angles are based on the engine centerline being located one engine diameter from the side of the fuselage, which was found to be an acceptable compromise when considering USB efficiency and critical engine inoperable moments, again by Boeing (ref.6). The side flaps are directly linked to the USB flap and are therefore opened only during low speed USB flight. During high speed cruise, the flaps are closed to decrease drag and increase aerodynamic efficiency.

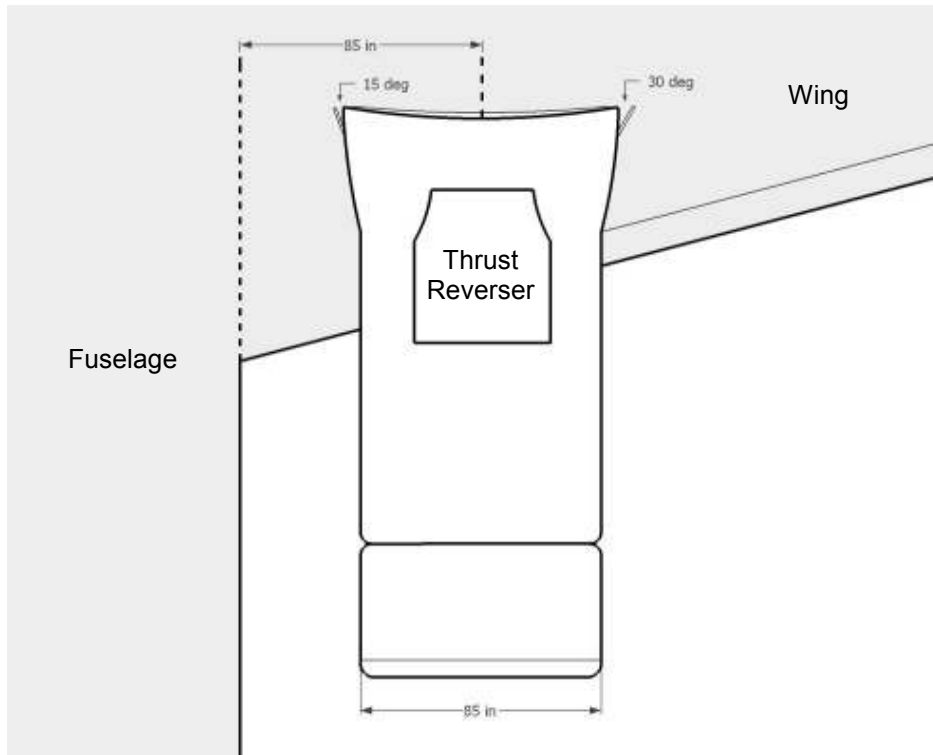


Figure 8-3: Overhead View of Exhaust Nozzle with Fully Extended Side Flaps

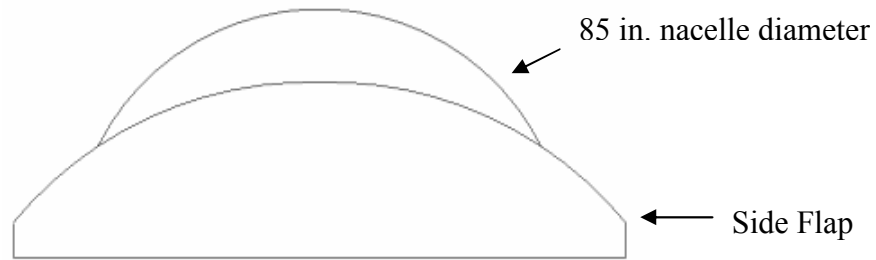


Figure 8-4: Rear View of Hermes' 3.5 Aspect Ratio D-nozzle

Hermes' engines are also equipped with a simple thrust reverser as pictured from above in figure 8-3. This feature is taken from the YC-14 research, in which this type of thrust reverser was proven to have an entire order of magnitude fewer parts than conventional systems (ref. 16). The thrust reverser is integrated into the engine nacelle and nozzle and can be quickly rotated during landing. The reverser flips downward into the flow and meshes against the upper wing surface to redirect the engine flow up and forward during braking and ground maneuvering. The forward component of the redirected thrust slows the plane while the upward component acts against the lift and therefore applies more weight to the tires for braking (ref. 16). This will help significantly with short landing applications.

8.4 Engine Removal and Maintenance

Ease and cost of maintenance were also important in designing the propulsion system features for this aircraft. By its nature, a USB design keeps the engines safer from debris ingestion as well as ground collision damage than a conventional low-mounted engine which in turn decreases lifetime maintenance and cost (ref.9). However, due to strict regulations on the number of hours an engine can fly before being overhauled, it is also important that engines can be removed quickly and easily when it becomes necessary, to keep the aircraft fully operating in the fleet. Since the engines are located forward of the wing spar, engine removal in a USB configuration is relatively simple. In a method often implemented on USB designs (ref. 16), Hermes has a removable inlet and hinged cowl doors as pictured in figure 8-5. Once the inlet has been removed, the cowl doors can be opened and the engine can be dropped out of the assembly with assistance from a crane and ground support vehicle.

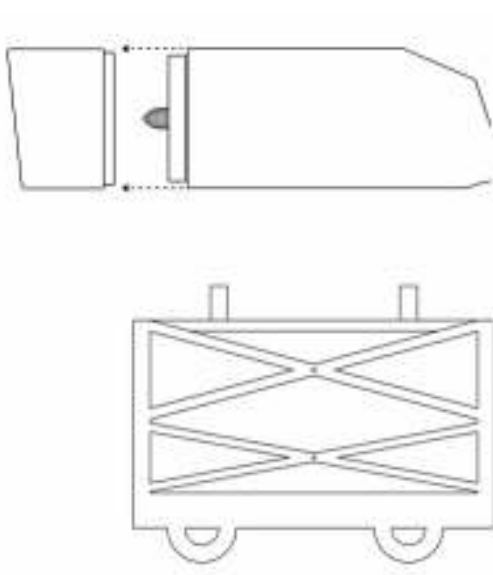


Figure 8.5.1

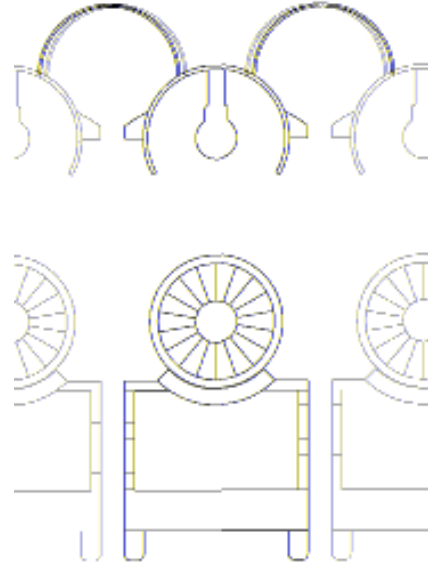


Figure 8.5.2

Figure 8-5: Engine Removal Method

8.5 Noise

When operating in austere and hostile environments, low noise output is a major benefit in the survivability of an aircraft and the success of the mission. Several USB noise tests have been conducted by NASA Ames in the Quiet Short-Haul Research Aircraft Flight Research Program (ref. 7). The findings of this research show that for an USB configuration, the noise footprint can be significantly smaller than a conventional layout, particularly during spiraling takeoff trajectories. The studies also found that most of the noise is generated at the trailing edge of the USB flap and that a sawtooth flap can further decrease the environmental noise footprint. The design layout of Hermes is similar in many aspects to that of the QSRA and so it is expected that noise levels will be well below all MIL and FAR regulations.

8.6 Additional Features

Several vortex generators are located behind the nozzle, near the trailing edge of the wing, as seen in figure 8-6, to energize the boundary layer by mixing the exhaust flow with the local boundary layer. The

vortex generators help to delay separation over the USB flap and are only extended at low speeds when the USB flap is in full use (ref. 16). When not engaged, the flaps sit flat against the upper surface of the wing.

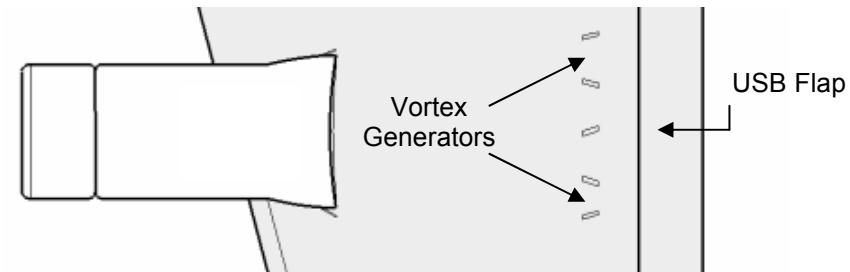


Figure 8-6: Top View of Vortex Generators on Wing Surface

9 Stability and Control

Static and dynamic stability describes the behavior of the aircraft. Analysis of static stability reveals positive stability and dynamic stability is required to determine the handling qualities of the aircraft.

Below are the flight conditions that each phase of the mission was determined by.

Table 9-1: Flight Conditions

	Take Off	Cruise	Landing	
Mach	0.2	0.8	0.2	---
Speed of Sound	1115.5	971.1	1115.5	ft/s
Density	0.002377	0.000737	0.002377	slugs/ft ³
Viscosity	3.7372e-7	2.9827e-7	3.7372e-7	---
CG	41.6	42.2	42.9	---
C _L	3.1	0.45	4.0	---

9.1 Tail Sizing

Hermes was designed with a high wing mounting and upper surface blowing, which requires a high T tail configuration to keep the horizontal tail out of the downwash. A goal was to trim the tails to the minimum area, decrease the structural weight and skin friction drag of the aircraft, while maintaining sufficient control power and maneuverability. Preliminary sizing was done using volume coefficients of typical jet transport aircrafts taken from Raymer (ref. 34) and Roskam (ref. 40). Sizes were then modified to resemble aircrafts with similar mission and configurations. Final sizing was done by evaluating the stability and control derivatives.

Table 9-2: Wing and Tail Characteristics

	Wing	Horizontal	Vertical	
Airfoil	SC(2)-0710	NACA 0012	NACA 0013	---
Area	2528	714	554.48	ft ²
Span	150	59.5	23.9	ft
Avg Chord	16.1	12	23.2	ft
MAC	19.15	12.45	23.2	ft
Aspect Ratio	8.9	4.96	1.03	---
Taper Ratio	0.259	0.5	1	---
LE Sweep	20.14	20	25	deg

The main drivers when sizing the vertical tail, was the need to land in a 25 knot crosswind and ability to handle asymmetric flight conditions, of an engine out scenario. The tail must be able to cancel out the yawing moment created by the engine thrust and wingspan at low airspeeds. The vertical tail was designed to have low sweep to keep the horizontal tail high, more forward, and out of the downwash.

Typical horizontal tail sizes of jet transports are between 25% and 40% of the wing area. Hermes horizontal tail size is 28% of the wing, keeping down the structural weight, while being able to achieve $C_{L_{max}}$ and provide a positive pitching moment at low airspeed and high thrust. This will ensure that the aircraft is capable of lifting the nose at takeoff.

9.2 Control Surface Sizing

The primary control surfaces, the rudder, elevator, and aileron were sized based on chord ratios found in Raymer (ref. 34). Flaps were sized based on comparative aircraft and the geometry of the wing.

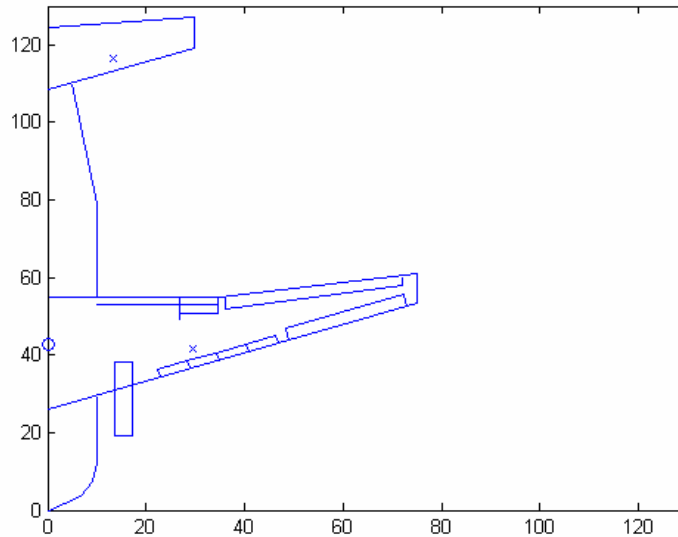


Figure 9-1: Wing Planform Control Surfaces

Due to having upper surface blowing, Hermes will have a single hinge USB flap inboard on the wing behind the engine. Outboard of this USB flap on the trailing edge is a double hinge flap, and an aileron. The aileron spans 90% of the outer portion of the wing near the wingtip for the purpose of creating a bigger moment, which would require less force to roll the aircraft. Aileron power was increased by increasing the chord length until sufficient control was established. The leading edge of the wing is similar to that of the Boeing 747 with four two by six foot Krueger flaps, which can increase the area of the wing producing more lift. Outboard of the Krueger flaps is a double hinge flap, to increase maneuverability and aid in takeoff and landing performance with high lift coefficients. Leading edge flaps also prevent the leading edge from stalling at the high lift coefficients. The control surfaces were evaluated by JKay VLM (ref. 20) to determine the authority needed to control the aircraft throughout the various flight phases of the mission.

Table 9-3: Wing Control Surfaces

	Chord, ft	Area, ft ²
LE Krueger	2	48
LE Flap	2.24	57.25
TE FLAP	3.04	24.32
TE Aileron	3.25	117.0

Across the entire leading edge of the aircraft, is a boundary layer control system. This system will generate higher lift coefficients and symmetric lift augmentation during an engine out scenario. The air is cross ducted from one engine to the other and when the flaps are extended, engine bleed air is directed over the leading edge to avert stalling and improve lift.

Table 9-4: Tail Control Surfaces

	Chord Ratio	Chord, ft	Area, ft²	Deflection, °
Rudder	0.35	8.12	145.73	35/35
Elevator	0.3	3.59	93.34	20/20

The rudder was modeled similar to the Boeing 727, to provide a large control force at low speeds. Size was dominated by the need to counter the yaw moment resulting from an inoperable engine. This scenario was analyzed at takeoff, under conditions of one failed engine at 1.2 times the stall speed specified by FAR 25.149

(ref. 39) with remaining outboard engine at max thrust and bank angle less than 5°. This scenario was evaluated using a FORTRAN program LDstab (ref. 8), which verified Hermes could handle an engine out scenario. No more than 75% of the yaw or roll control was allocated to compensate for the asymmetric loss of thrust. The rudder is 84% of the span of the vertical tail, with a chord ratio of 35%.

Elevators create a downward pressure which counters the moment of the center of gravity pivoting around the aerodynamic center. Hermes elevator is 90% of the span of the horizontal tail and is capable of producing a nose up pitching moment at takeoff.

9.3 Longitudinal Static Stability

Longitudinal static stability is concerned with the aircraft's pitching moment coefficient for stick fixed conditions. Hermes is statically stable during all flight phases. The static margin at takeoff is 27%, providing a positive pitching moment. The longitudinal stability derivatives were calculated using the FORTRAN program JKay VLM (ref. 20) and can be found below.

Table 9-5: Longitudinal Stability and Control Derivatives

	Take Off	Cruise	Landing
$C_{L\alpha}$	4.8725	6.00554	4.86853
C_{Lq}	11.14421	12.19028	10.1206
$C_{m\alpha}$	-1.31581	-0.92356	-0.80844
C_m/C_L	-0.27005	-0.15378	-0.16606
C_{mq}	-39.137	-43.8188	-36.8765
$C_{L\delta e}$	0.33618	0.37547	0.33618
$C_{m\delta e}$	-1.3645	-1.52201	-1.32939

9.4 Lateral/Directional Static Stability

Lateral static stability refers to the rolling motion of an airplane due to sideslip. Hermes is laterally stable; because when the aircraft is sideslipping a roll moment arises that diminishes the bank angle ($C_{l\beta} < 0$). Lateral stability was increased by mounting the wings high on the fuselage, sweeping the wings, and by placing the wings at a dihedral. Hermes was designed with a big horizontal tail that was placed as far back from the center of gravity as possible to increase static stability.

Directional static stability refers to the yawing motion of an aircraft due to sideslip. Hermes is directionally stable since yawing moment increases with increasing sideslip angle, creating a positive yawing moment. Hermes is directionally stable. Positive sideslip is defined as left of the nose from an aerial view of the aircraft. Static directional stability was increased by increasing the size and the moment arm of the vertical tail, which increasing the yawing moment coefficient. The lateral and directional stability derivatives were calculated by JKay VLM (ref. 20) Fortran program.

Table 9-6: Lateral/Directional Stability and Control Derivatives

	Take Off	Cruise	Landing
C_{lp}	-0.54019	-0.67940	-0.54019
C_{np}	-0.50079	-0.52729	-0.5006
C_{yr}	0.3942	0.41118	0.3839
C_{lr}	0.04285	0.04461	0.04174
C_{nr}	-0.16588	-0.16906	-0.15666
$C_{y\beta}$	-0.38606	-0.40663	-0.38606
$C_{l\beta}$	-0.04203	-0.04524	-0.04203
$C_{n\beta}$	0.15098	0.15449	0.14587
$C_{l\delta a}$	-0.3525	-0.44519	-0.3525
$C_{n\delta a}$	-0.00062	-0.00047	-0.00135
$C_{l\delta r}$	0.02951	0.02958	0.02951
$C_{y\delta r}$	0.27222	0.27276	0.27222
$C_{n\delta r}$	-0.12849	-0.12775	-0.12486

9.5 Dynamic Stability

To achieve dynamic stability, Hermes must meet the military specifications for flying qualities of piloted airplanes, set forth by MIL-F-8785C (ref.22). Hermes is considered a Class II aircraft which will encounter categories B and C flight phases during its mission. With calculated moments of inertia, the handling qualities of Hermes could be evaluated. With out the moments of inertias, only the dimensional stability derivatives could be calculated. However Hermes was able to meet the Class II requirement for spiral stability ($L_{\beta} N_r - N_{\beta} L_r > 0$). The dimensional stability derivatives were calculated by methods found in Roskam (ref. 40).

Table 9-7: Dimensional Stability Derivatives

Y_r	0.0156454	0.00541	0.017089	ft/sec
Y_β	-0.045578	-0.05542	-0.05112	ft/sec ²
Z_α	-0.590004	-0.82456	-0.67413	ft/sec ²
L_β	-0.000231	-0.02011	-0.0173	1/sec
L_r	7.915E-05	0.001914	0.005776	1/sec
N_β	0.0003054	0.040641	0.03554	1/sec ²
N_r	-0.000113	-0.00429	-0.01283	1/sec
M_q	-3.18E-06	-5.4E-05	-0.00019	1/sec
M_α	-8.8E-05	-0.00525	-0.00525	1/sec ²
$M_{\dot{\alpha}}$	-3.18E-06	-5.4E-05	-0.00019	1/sec

9.6 Flight Control Systems

For the flight control system, initial consideration was given to a hydromechanical, power by wire, and fly by optic system. The hydromechanical system was almost immediately eliminated due to the increases in weight and maintenance. With the increase in weight comes an increase in cost as well. The mechanical and hydraulic system would also require more maintenance, due to lubrication, tension adjustments, leak checks, and fluid changes. However hydraulic actuators will be used in combination with a digital fly by optic control system. This eliminates the hydraulic circuits with electrical circuits, allowing the system to become smaller in size and weight. The electrical interface will take the pilot's input and determine the best means of providing the desired response by moving the actuators at each control surface. The electrical circuits can also provide improvements in safety, by responding to changes in aerodynamic conditions and can prevent stall and overstressing of the frame as well. The system will have redundant power circuits for increased reliability. The fly by optic system is being used, because of the systems ability to transfer data at higher speeds and it's immunity to electromagnetic interference and weaponry by use of fiber optic cables. With the fly by optic system there is no need for heavy metallic shielding of the system, while retaining all the benefits of a digital fly by wire system.

Another system is the stability augmentation gust alleviation system (SAGAS). The SAGAS system is capable of independently actuating control surfaces to counter any disturbances and induced oscillatory motion. It can trim the aircraft to fly as it becomes less stable with weight reduction and center of gravity travel due to fuel consumption.

9.7 AVL Model and Assumptions

An accurate vortex lattice modeling of Hermes was instrumental to predicting its aerodynamics, stability, controls, and resulting performance. With the location of the center of gravity in place, including CG travel during the mission, the lifting and control geometry was modeled in the vortex lattice code AVL® developed by Professor Drela at MIT (ref. 20). Using only the designed lifting surfaces, the following model is a precise replica of Hermes in 3-dimensions:

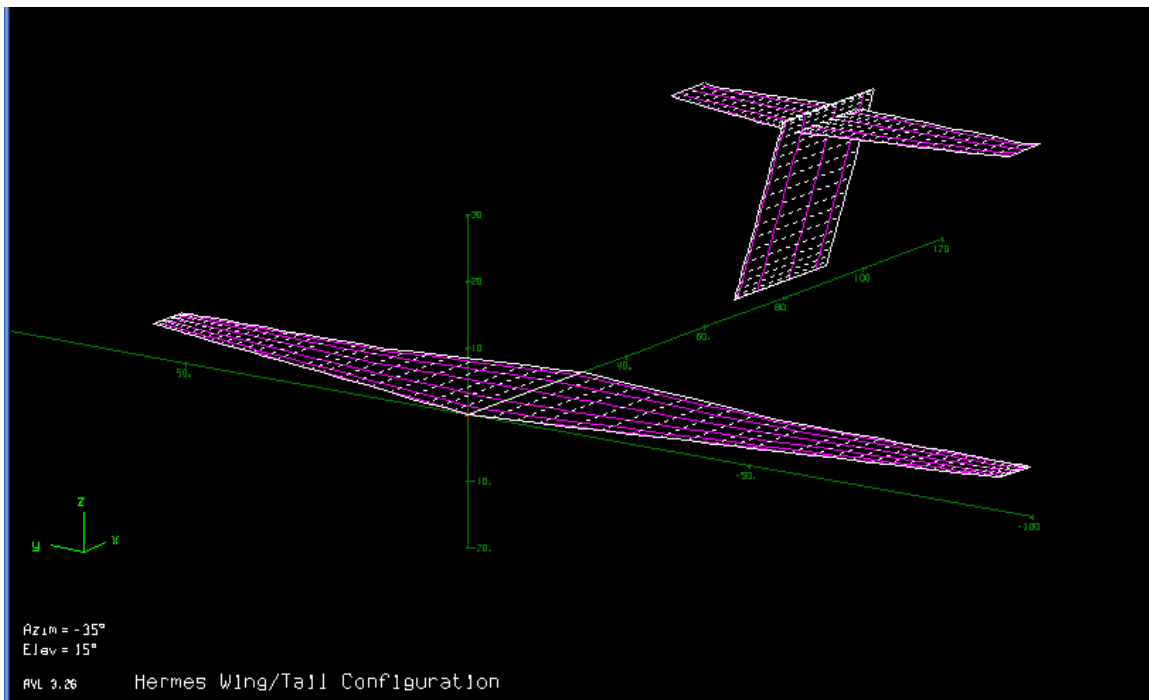


Figure 9-2: Hermes 3-D

The spanwise horseshoe vortices can be seen as the dotted lines running the chord length of each lifting surface. Panels were grouped near the wing tip to get a more accurate estimate of induced drag. For

the tail configuration, panels were loaded near the points of projected interference; the intersection of the two tail components. AVL also took in as input our supercritical and symmetric airfoil coordinates for the lifting surfaces, allowing more accurate lift curves to be developed at the variable flight conditions.

Some key assumptions were made during the sessions. It was assumed that our wing and tail configuration, coupled with the specified control surfaces, would dominate the aerodynamic forces of the aircraft. Calculations at cruise conditions were a concern as well. AVL is a good estimate up through our transonic cruise speed, where the Prandtl-Glauert compressibility correction is still a decent estimate but fails soon after. Our vertical CG will shift a small amount during flight, but only the length-wise shift of CG will be assumed to change. It was also assumed that Hermes would produce symmetric lift and that the pitching moment would be the chief threat to a successful take-off. The most important conjecture is the effective increase in spanloading due to the USB configuration is such that the lifting configuration meets the $C_{L_{max}}$ requirement less the effective increase in lift loading due to said high-lift technologies and also helps to preserve an elliptic-like spanloading. It has already been shown that the mechanical and powered lift devices being employed by Hermes can produce wing lift coefficients upwards of 6, so these assumptions will hold for the purposes of the preliminary design.

Table 9.9 gives Hermes' preliminary trimmed conditions during the primary flight conditions. These results were compared and matched with other aerodynamic calculations which are summarized in the Aerodynamics section.

Table 9-8: Hermes 3-D

Constraint/Result	Climbing at Takeoff Value	Straight & Level Cruise Value	Descent at Landing Value
C_L	1.5	0.45	2
C_M , pitch	0	0	0
Velocity	190 fps	770 fps	120 fps
Density	0.002378 slugs/ft ³	0.000737 slugs/ft ³	0.002378 slugs/ft ³
Mach	0.171	0.8	0.107
CG location	15.69 ft. aft wing LE	16.89 ft. aft wing LE	17.69 ft. aft wing LE
Elevator Deflection	-20.15	1.1952	-25.26
Efficiency	0.9616	0.857	0.9832
Angle of Attack	13.5	-1.08	19.88
C_{Di}	0.08651	0.00847	0.1544
C_{Dp}	0.04	0.02	0.045
C_D	0.1212	0.0249	0.1842
NP	28.63 aft wing LE	25.99 aft wing LE	29.47 aft wing LE

10 Materials and Structures

10.1 Materials

Several different kinds of materials were researched in order to know all available to be used. Al 2024 was commonly used in early planes and since has been a basis model for estimating weights (ref. 36). Aluminum alloys are still commonly used in planes today. Composites are being used more and more, as they allow for a greater strength and reduction in weight. This, however, is offset by their cost.

Many materials are used in aircraft today. They include carbon-fiber reinforced plastic, glass-fiber reinforced plastic, titanium alloys, and glare.

Glare is a sandwich of materials. It has an aluminum alloy for the bread and the inside is fiber-glass. The number of layers can be changed, most have two aluminum and one fiber-glass. Additional layers of each have been added in a few cases, making the ratio three to two. Several different kinds of aluminum alloys can be used, the most common one that I have found has been the alloy 2024 T-3. I am sure that several different kinds of composites can be used as the inside, however, all I have found thus far has been fiber-glass as that constituent (ref. 31).

Table one shows a list of materials their densities, strengths, and lists where the material is used by two other planes.

Table 10-1: Materials (27, 13, 32, 29)

Material	Density (lb/in ³)	Yeild Strength (ksi)	Tensile Strength(ksi)	A-380	Euro A-400
Al 2024	---	50	70	---	---
Glass fibre reinforced plastic	0.066	---	87	Wings, tail, fuselage sections	Light loaded areas
Ti-5 Al2.5 Sn		110	115	---	High loaded areas
Glare	0.091	---	156	Upper Fuselage	---

Glare will be used for the skin of the aircraft, including the struts. This is for the ease of repair associated with Glare. Glass fibre reinforced plastic will be used in the interior structures of the aircraft, because of its extra strength and light weight. Titanium will be used to help with the loads on the landing gear. All of these are subject to change in the future as better materials become available.

10.2 Weight Reduction

Since the basic weight was determined using Roskam's book the weight is slightly incorrect. This is because it uses the aluminum 2024 as its basis. As can be seen in Table 10.1 the density is the second greatest in the table. Since the other materials are less dense and the weight of the structure will be decreased just by the use of the new material. In Table 10.2 shown below, Roskam shows an example of weight reduction fractions.

Table 10-2: Weight Reduction Numbers

Primary structure	Composites	ARALL	Al-Li
Fuselage	0.75-0.85	0.75	0.9
Wing, tail	0.75	0.75	0.9
Landing Gear	0.88	N/A	0.9
Secondary Structures			
Flaps slats	0.7	0.8	0.9
Air induction System	0.7-0.8	0.75	0.9

By changing the entirety of the structure from aluminum 2024 to the new material you may then multiply this number by the 2024 weight; giving you a reduced weight. The use of the Al-Li gives a weight reduction of about 10%. Using this as a guide as well as the densities given in Table 10.1 a rough estimate of the weight reduction is about 15%. This number may increase or decrease as any future materials are used in place of the current ones (ref. 36).

10.3 Struts

The struts of the Aircraft are used to allow the wing to have a greater aspect ratio, as well as a thinner wing. These features allow for a decrease in induced drag and transonic wave drag. The thinner wing also provides for a decrease in the wing sweep. This decrease in wing sweep along with the increased aspect ratio gives the wings a more natural laminar flow over the wing (ref. 33).

The struts will be melded into the wing at a 90 degree angle. This creates less interference drag. The strut will also be designed to have a slack distance. This distance will be about 5% of the cruise wing loading. This will ensure that the strut does not activate during negative load maneuvers, where the extra strength needed to keep the strut from buckling would make it useless as a weight reduction technique for the wing. The slack will also allow the strut to become more active as the load increases on the wing. This sleeve for the extra slack can easily be seen in figure 10.1.

The placement of the strut on a wing with an engine mounted on the underside of the wing shows best performance at $\frac{3}{4}$ the length of the wing. This would follow suit for an engine mounted on top of the wing, as the weight placement and therefore moments are nearly the same (ref. 33).

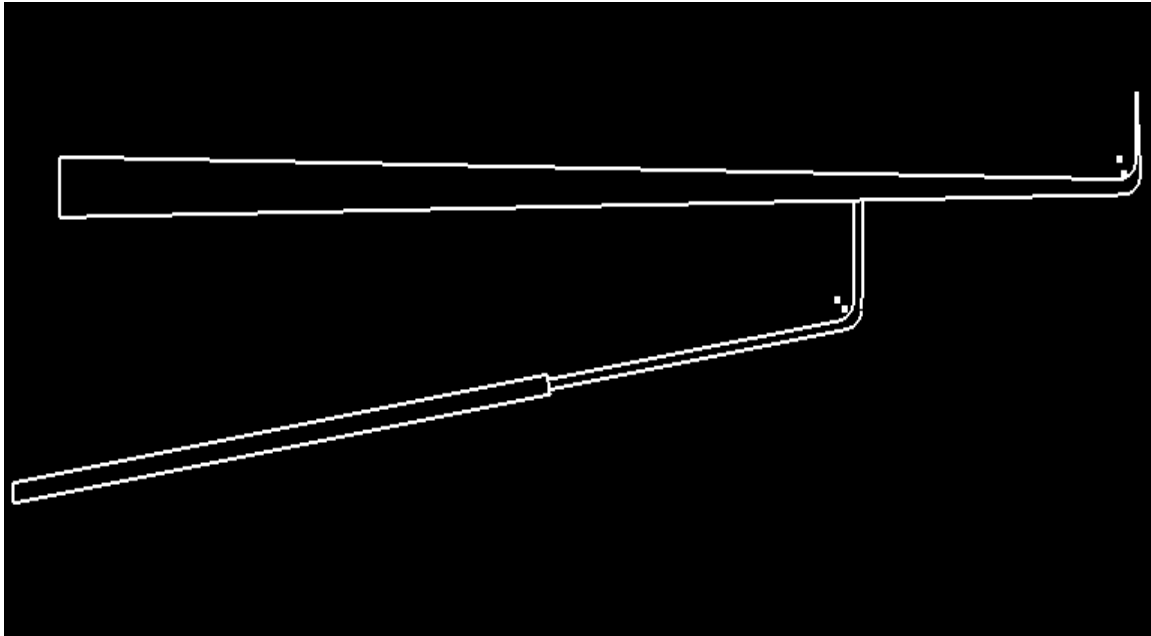


Figure 10-1: Wing and Strut

10.4 Wings

The wings internal structure is based of off cutaways found of similar transports (ref. 45). This places a wing rib at every end of the control surface. This is shown in figure 10.2. Knowing where the control surfaces are allows the placement of the stringers and the spars. The first spar will be located at about 12% of the chord length from the front, and about 30% of the chord length from the back. The spars run along the in a direction that will allow for a maximum allowance for space for the wing box while not interfering with control surfaces. Figure 10.3 shows the wing box and the airfoil. The stringers are an integral blade section. This is a widely used way to stiffen the panels. The blades will run about every 0.4% chord from spar to spar. The front spars and rear spar are marked by the edge of the red line outlining the wing box within the airfoil.

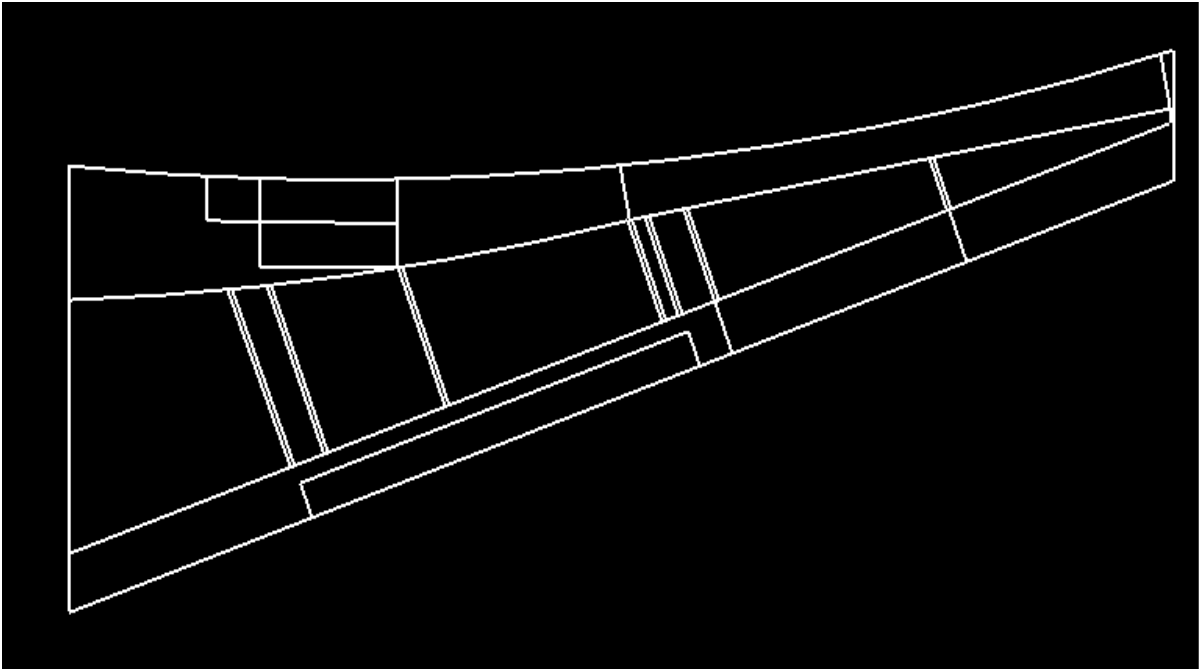


Figure 10-2: Wing Section

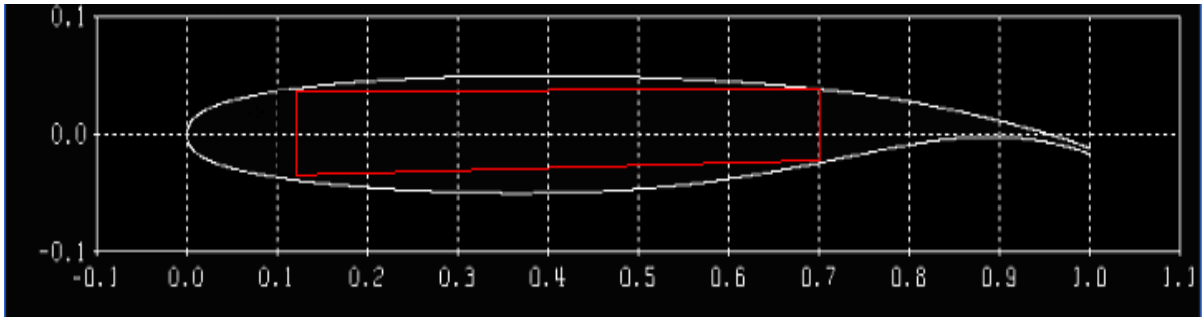


Figure 10-3: Wing box

Over 50% of the wing volume is still available for use. This allows for fuel to be placed into the wing.

10.5 Fuselage

The fuselage calculations were very similar to the wing. Using reference 26 and having 30 stringers gave an area for each stringer to be 6.05 in^2 , excluding the four stringers closest to the 0 and 180 degree points on the circle that is the fuselage, they have an area of 8.08 in^2 . Figure 10.4 shows the stringers as a circle along the edge of the outer skin on the far left. It also includes a representation of the skin on its own in the middle and a representation of the rear pressure bulkhead on the left. This bulkhead can be seen to move upward to allow the cargo to be loaded and unloaded.

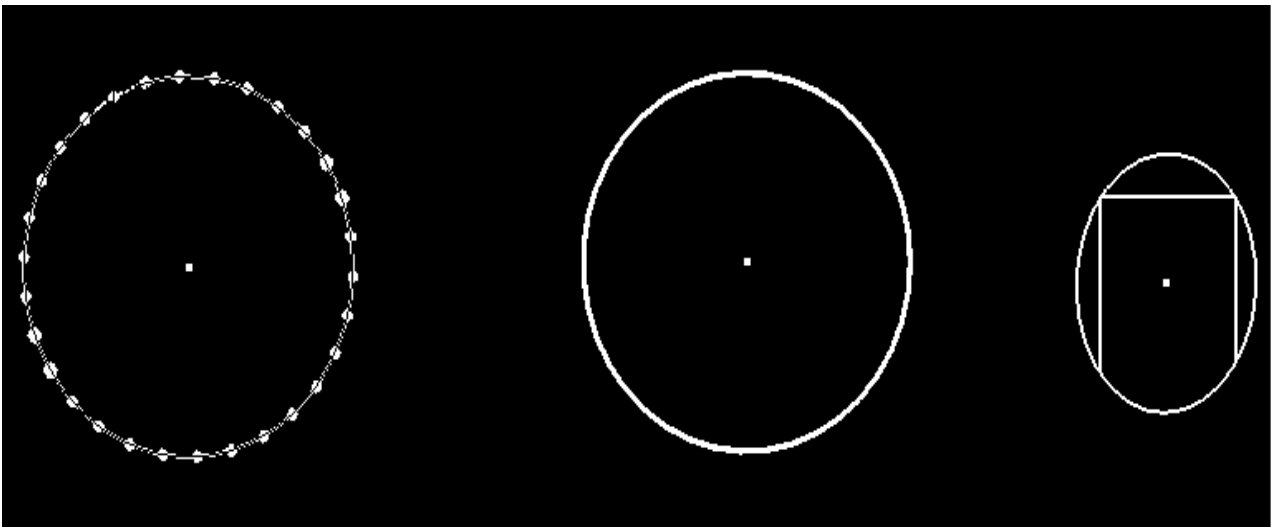


Figure 10-4: Fuselage stringers, skin, and pressure bulkhead

Using similar transports cutaways to find where the frames would be placed (ref. 45), shows several placement of frames. The frames would be placed to separate the cockpit area from the cargo area. There would be four frames surrounding the wings. One on each side of the wing, and then one on the inside edge of the forward and rear control surfaces. Another frame will be placed at the bottom edge of the loading door. At the top edge of the loading dock, another section of the tail will move upward into the tail section. At this point there will be another frame. This totals at 6 frames, shown in figure 10.5 and 10.6.

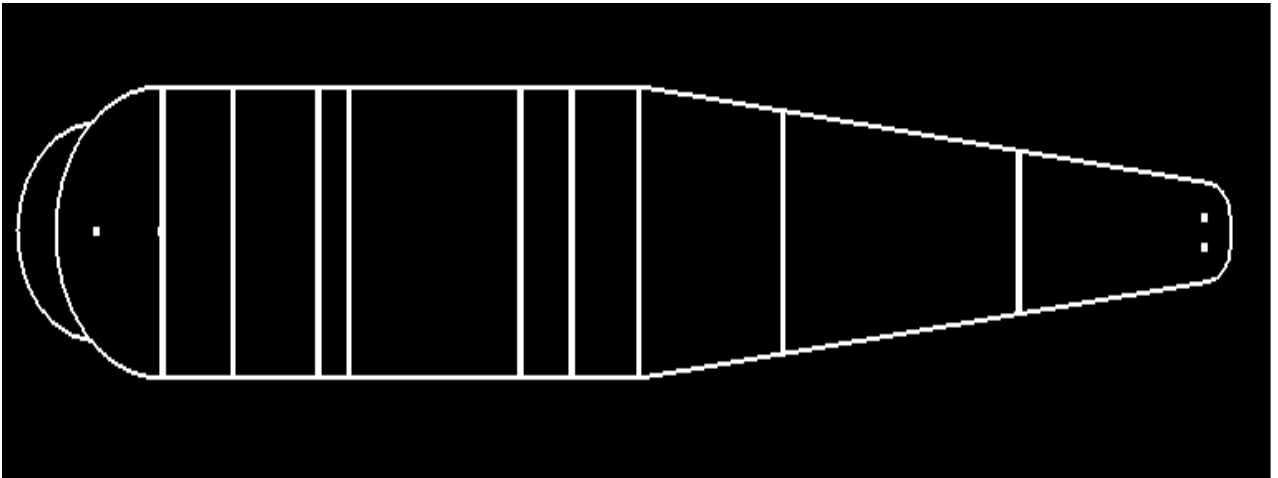


Figure 10-5: Fuselage (topview)

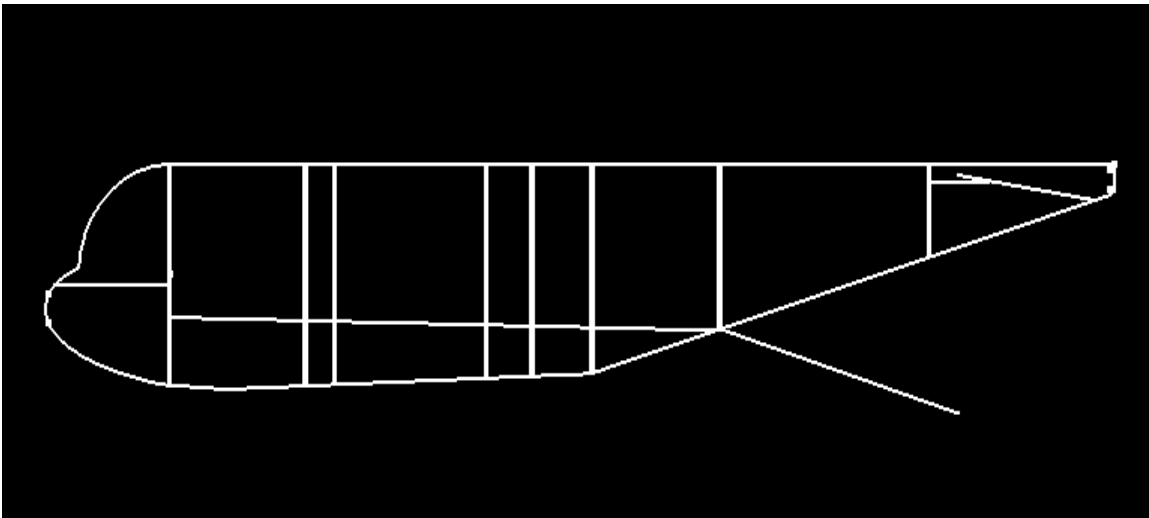


Figure 10-6: Fuselage (sideview)

As can be seen in figure 10.6, the floor of the space is raised to make room for the landing gear. The rear hatch is separated into two different sections, one section that moves downward to make a ramp for the cargo to be loaded or unloaded and the other moves upward into the tail section in order to make room. The pressure bulkhead has a section that moves upward as well to make clearance for the cargo as well. The main floor for the cockpit is shown as well.

10.6 V-n Diagram

The V-n diagram in Figure 10-7 represents the loads Hermes is expected to bear during the required missions. The load limits of +3 and -1 vertical g's is a standard range for a transport aircraft. With a safety factor of 1.5, Hermes has an ultimate load factor range of +4.5 and -1.5 vertical g's. The RFP required a maximum design cruise speed of at least Mach 0.8 at an altitude of at least 30,000 feet; these requirements are reflected in the V-n diagram. The gust envelope does not exceed the flight envelope at any point. The gust envelope does exceed the limit load in the dive speed range, this is beyond the maximum design cruise speed and so, by definition, outside the flight envelope. Therefore, Hermes does not require structural reinforcement for gust loads.

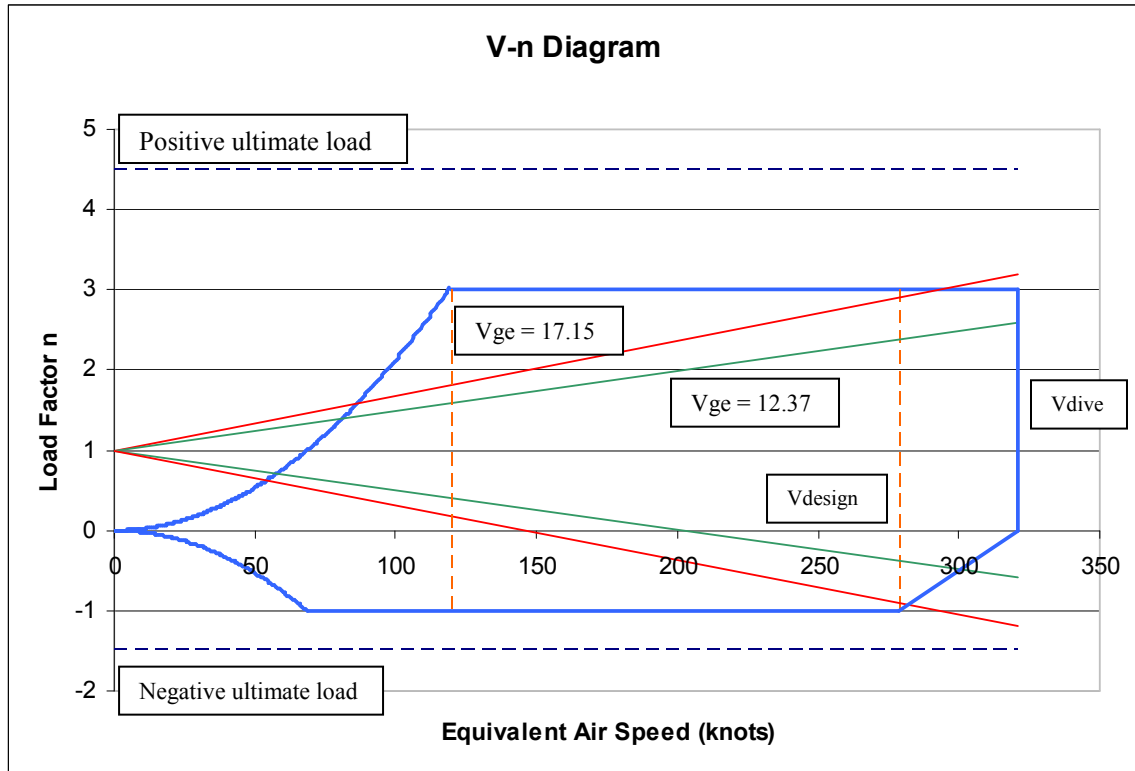


Figure 10-7: V-n diagram for Hermes

11 Systems

Hermes is equipped with much of the same systems as used by today's flying military transports with the addition of a few experimental avionics. The systems chosen were done so for mission success and safety. The layout of Hermes is provided in figure 11-1.

11.1 Cockpit

Hermes has the basic avionics military transports need and the radios required to successfully complete the missions required by the RFP. Most of these components are taken from existing aircraft to help reduce production costs. The cockpit display with a description is given in figure 11-2. Some of the avionics includes secure voice and jam resistant UHF/VHF/HF, SATCOM, VHF AM/FM. An identification friend or foe system is implemented. Pilots also have a wireless intercom system (ref. 1).

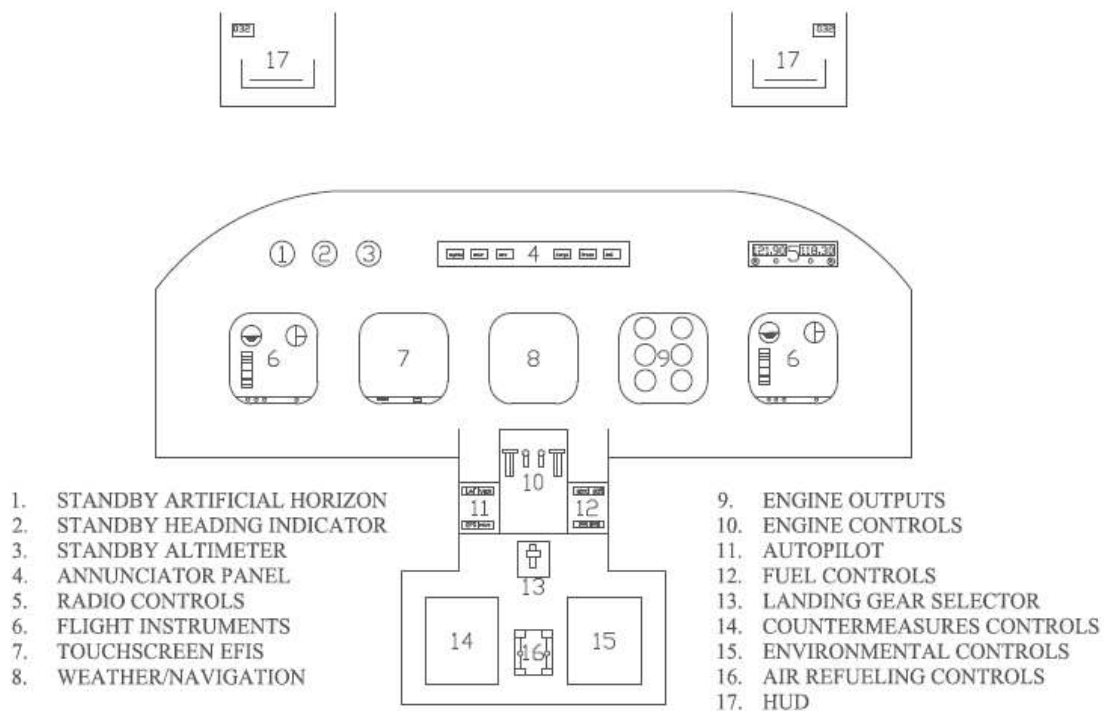


Figure 11-1: Cockpit in Hermes aircraft

The RFP states the aircraft must be able to takeoff and land in all weather conditions. A mostly glass cockpit is ideal for ease of use and uniformity among other newly designed aircraft. The pilot and co-pilot will have multi-functional displays directly in front along with a heads-up-display. Navigational capabilities are required of the RFP and the Garmin G1000 is well suited for this mission. The G1000 has

approved dual integrated radio modules that allow the aircraft to have oceanic navigational capabilities. The G1000 also has very high frequency (VHF) navigation and instrument landing systems (ILS) that permit the aircraft to approach for landing in inclement weather conditions (ref. 15). Hermes has a touchscreen en-flight information systems (EFIS) for ease of use.

Hermes is required by the RFP to fly at low altitudes to complete the mission in hostile areas. Thus, the aircraft will need highly reliable capabilities to avoid controlled flight into terrain. Hermes navigational software is updated with L-3 Communications' Military Airborne Surveillance System (MASS) (ref. 28). This system gives Hermes an enhanced surveillance volume, the ability to rendezvous and fly formation with up to fifty aircraft. It allows includes Traffic Collision (TCAS), and terrain awareness (TAWS) in one package which lowers the costs. Terrain Avoidance Warning System has a database of the earth's terrain and allows the aircraft to fly relatively close to the surface and will give audible warnings as well as providing evasive maneuvers if necessary. TAWS capabilities will help during takeoffs, landings, and avoiding enemy identification. The system does not provide any forward electronic emissions. MASS complies with all ATC requirements for integration into civilian airspace.

11.2 Lighting

Hermes has formation lighting for safely clustering with other military aircraft. It also has standard anti-collision lighting for civilian integration. High intensity strobe lights are also provided on each wing tip for safety during non-military operations. Landing lights and taxi lights are provided on the nose, wing tips, and mid-span. Figure 11-3 is a layout of the lighting on Hermes.

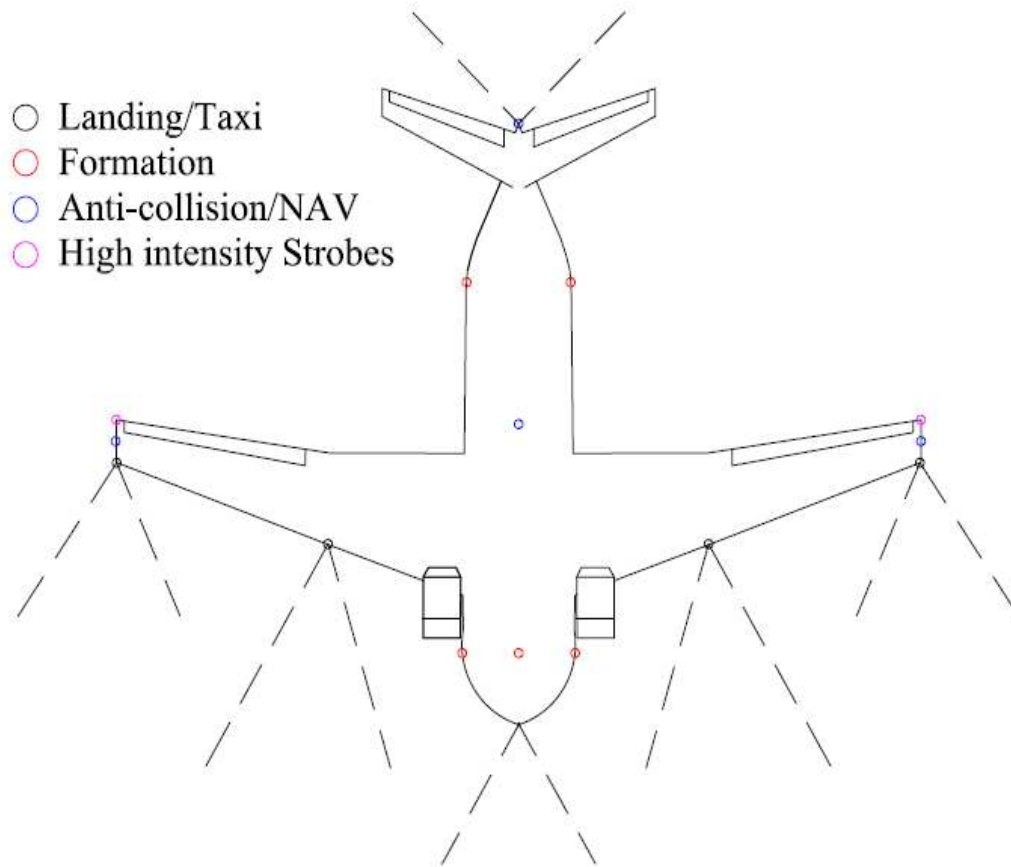


Figure 11-2: Hermes lighting configuration

11.3 Fuel System

There are three fuel tanks located one in each wing and one above the cargo bay in the fuselage. The mission requires 640 ft³ of fuel with full payload. The tanks are almost 810 ft³ in volume so they will hold more than required but should not be topped off when flying with full payload. Because the aircraft will likely be flying into and out of war zones, the fuel tanks are self-sealing fuel bladders that prevent and close off leaks should the tanks get hit with small arms from enemy forces. For the secondary mission, in-flight refueling is provided for extended flights. In-flight refueling is provided to the center tank and a fuel pump transfers fuel from center to wing tanks. The fuel tanks and lines are shown in figure 11-1.

11.4 Landing Gear

Hermes uses a tricycle type landing gear arrangement with two wheels per strut including the nose gear. This arrangement has been chosen using *Aircraft Design: A Conceptual Approach* by Raymer (ref. 34). Since only two wheels per strut are used for the main gear, larger tires had to be used. The main tires have a 47" diameter and an 18" width. The nose tires are 28" in diameter and 9" wide. These larger tires will help make smoother off field takeoffs and landings. The stroke was determined to be 3.88", also found using Raymer's method. The landing gear can be viewed in figure 11-4.

While some progress is being made with electrically actuated landing gear, Hermes is equipped with hydraulic actuators. A hydraulic system is used because of the landing gear size and weight. Hydraulic actuators are used due to their dependability and survivability proven in the field.

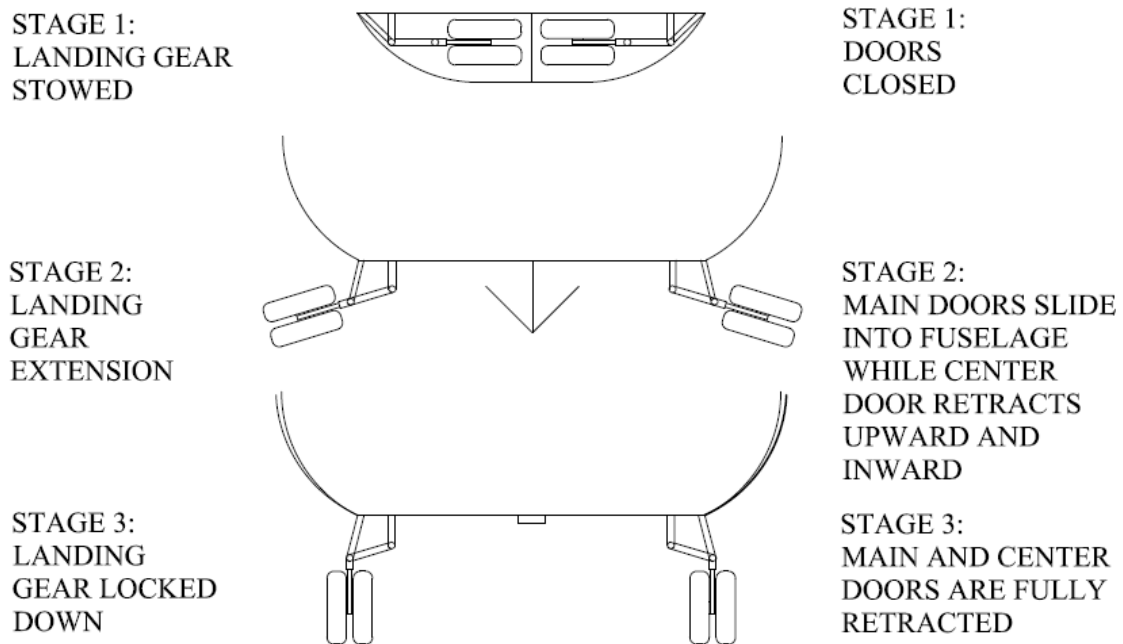


Figure 11-3: Hermes main landing gear

11.5 Shrink Shock Strut Summary

The automatic shrink shock strut is a type of landing gear in which the shock strut cylinder and a shock strut piston are mounted coaxially. In between the piston and the cylinder there are a host of chambers. They are the shock strut shrink chamber and a gas spring chamber. During retraction the system works by filling the strut shrink chamber with hydraulic fluid and filling the gas spring chamber with pressurized gas. Initially the pressurized gas forces some of the hydraulic fluid out of the hydraulic fluid supply and into the shock strut shrink chamber. In response the shock strut shortens in length. The mechanism works in reverse for the expansion of landing gear. The pressurized gas returns to the gas chamber thus forcing the hydraulic fluid back into hydraulic fluid supply.

12 Hermes Performance

The largest uncertainty in the conceptual design process is performance. Sections and components of an aircraft can be designed individually around certain constraints, but how well those individual pieces come together to meet the design requirements is fuzzy even with quality estimates. The following sections provide estimates and insight into the performance of the Hermes Concept.

12.1 Mission Program and Design Adjustments

With several details of Hermes' concept known, the initial step in performance evaluation is determining how much fuel will be used over the course of the mission. In preliminary sizing the range equation was used as a rough estimate for fuel usage. Using the AIAA engine deck and a more detailed aerodynamic model of Hermes as inputs, a Matlab based mission program written by Mike Morrow at Virginia Tech (ref. 30) gave the accurate mission-fuel breakdown. The original fuel weight estimate of about 36,600 lbs proved inadequate. For roughly 15% reserve fuel the total fuel weight had to be increased to 43,500 lbs, which gave 6,000 lbs for reserve purposes. Given our maximum volumetric fuel capacity of 47,000 lbs, this set-up will work. The final fuel breakdown for the primary mission is shown in Figure 4-1. One explanation for this inconsistency during sizing is the use of one fuel fraction for the return trip and not two; the low altitude run was assumed to be part of the high altitude cruise, which is more fuel efficient.

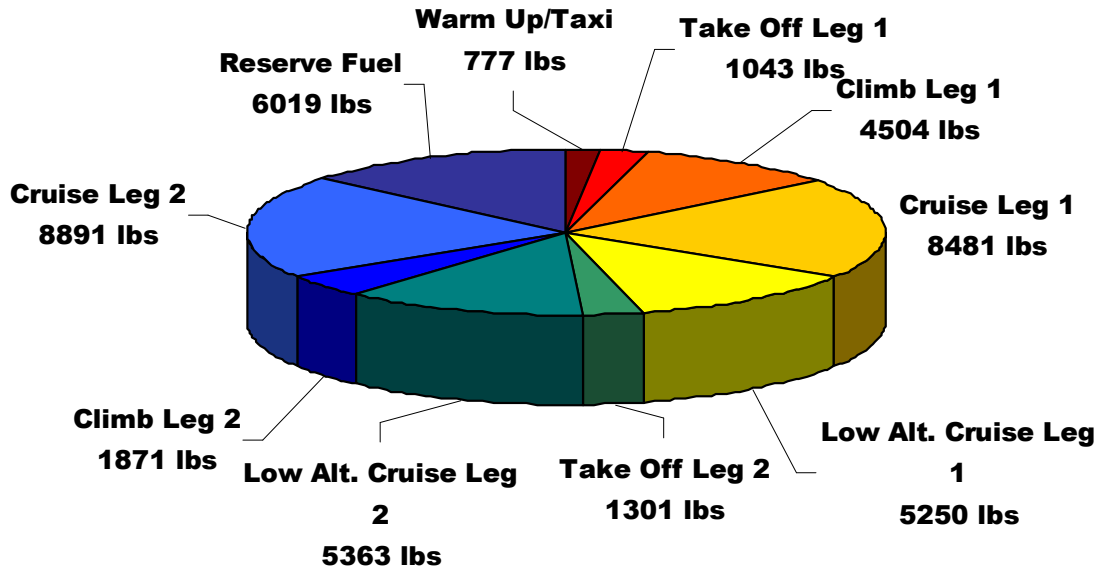


Figure 12-1: Primary Mission Fuel Breakdown

Adding over 3 tons to takeoff gross weight changes the field performance. A major assumption made in Section 4.2 was that a 10% empty weight decrease would be possible given current materials and structures; a conservative estimate. Employing advanced structures, such as struts, with superior composites and alloys makes a 15% empty weight reduction appear reasonable. Assuming this is possible, takeoff gross weight is marginally altered; 182,820 lbs. Up only 1,500 lbs from the sizing estimate, field performance should not be dramatically altered and the results from the original sizing shouldn't be affected. Additionally, this means that the aircraft will not have the capability to fly the entire 1200 nm mission radius with payload, but it will be able to re-direct several hundred miles to a safe landing zone. Another solution would be to find a cruise altitude other than 35,000 ft where Hermes is more efficient and uses less overall fuel.

12.1 Take-Off and Landing

Meeting a balanced field length (BFL) of 2,500 ft. is not easy to accomplish for most transport aircraft of any practical size. Balanced field lengths were calculated using the aforementioned take off and landing program (ref. 21). As Figure 12-1 shows clearly, BFL requirements were met on a standard day with a C_{Lmax} as low as 3.3. However, given the hot-day requirements, Hermes requires a C_{Lmax} of 4.8 to

meet the take-off obligation. Take-off distances, which included clearing the 50 ft. obstacle, were shown to fall between 150 and 200 feet shorter than their corresponding BFL's.

During preliminary runs of the program, it was shown that take-off distances, and hence BFL, started to increase with any maximum lift coefficient over the value of 5.5. Hermes created too much drag with higher lift coefficients, which hindered its short field performance, as predicted in the original sizing. Considering the fact that Hermes will be forced to deflect control surfaces to stabilize longitudinally, and also to counter strong crosswinds, reducing the amount of drag at the take-off configuration was a paramount concern in design. Another concern during take-off for Hermes was over-rotation at high lift coefficients, which would create uncontrollable pitching moments and likely result in a crash. In light of this, our design maximum lift coefficient of 4.5 was confirmed as a strong choice for a compromise between the short-field requirements, reduction of aerodynamic inefficiencies, and providing stability with ample control authority left over.

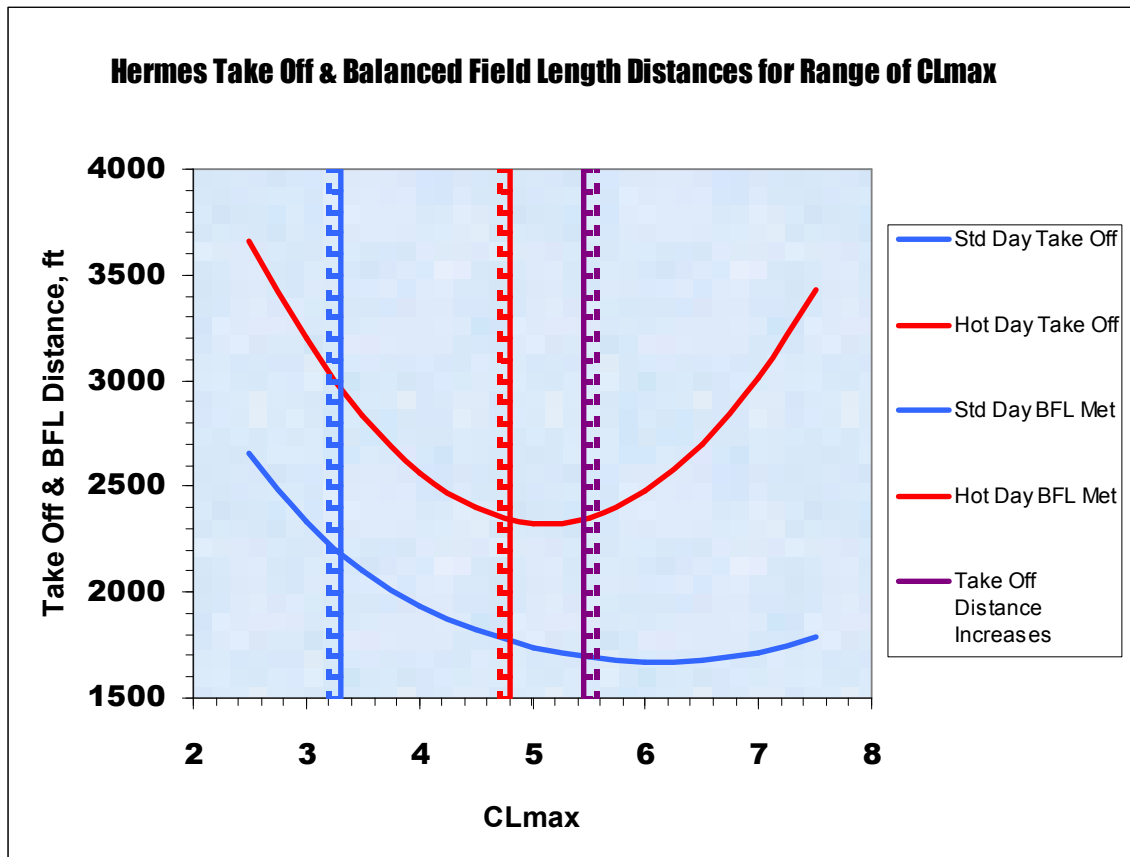


Figure 12-2: Hermes TO and Balance Field Lengths

Landing within the required balanced field length of 2500 ft. was not as difficult as taking off in the same distance. This is in part credited to the high lift coefficients generated by the Hermes' configuration and the low stall speeds, which averaged 65 knots for low speed, low altitude mission segments. The previously mentioned mission program also helped provide aircraft weights and thrust requirements on decent to landing. It was also assumed that Hermes could produce 15,000 lbs of reverse thrust during the ground roll on a standard day. Using the inputs outlined in Sean Lynn's report (ref. 21) Table 12-1 was produced.

Table 12-1: Hermes Landing Distances

Primary Mission	Emergency Landing	Payload Delivery	Mission End
Landing Distance	2376 ft	2398 ft	1437 ft
Landing Distance (Hot Day)	2694 ft	2497 ft	1521 ft
Ferry Mission	Emergency Landing	Mission End	
Landing Distance	1741 ft	1434 ft	
Landing Distance (Hot Day)	1970 ft	1567 ft	

The scenario for a successful mission will result in Hermes achieving its landing field requirement of 2,500 ft. with a C_{Lmax} of 5.5, given our assumptions. If the high-lift systems are inoperative, the landing distance for the mission is increased to 3,900 ft. unless fuel is dumped. An emergency landing, e.g. landing right after take off, can only be achieved by dumping fuel unless Hermes can approach with a C_{Lmax} higher than 5.5; a region where the designers are not comfortable to comment on. As the aircraft will weigh less at the end of the mission, our first landing segment was the chief constraint on landing field performance, where it was met for our current configuration. Given our volumetric fuel capacity constraint, Hermes will not be as heavy flying and can meet all landing field requirements with a lower C_{Lmax} . Hermes' landing distance was most sensitive to approach thrust, reverse thrust available, landing weight, and C_{Lmax} . A reliable and efficient high-lift system is the best way to ensure the field performance of Hermes.

12.2 Climb and Ceiling

Due to the rather short mission range, relative to other transports, the climb segment was important for several reasons. First, finding an efficient cruise altitude must be balanced with a sensible climb rate. If not balanced, Hermes can waste too much fuel climbing to an efficient cruise altitude, or could spend most of the mission segment climbing if it is too slow. Also, calculating climb helps determine service ceiling. Table 12-2 summarizes the maximum rate-of-climb results. Values for the climb on the return trip are shown in red.

Table 12-2: Climb Parameters

Altitude, ft	CGR_{max}	RC_{max}, fpm	Best RC Angle
0	0.222, 0.474	3074, 4777	12.83, 28.27
5000	0.192, 0.417	2862, 4528	11.08, 24.66
10000	0.133, 0.306	2139, 3582	7.65, 17.82
15000	0.099, 0.242	1719, 3058	5.68, 13.98
20000	0.068, 0.183	1282, 2516	3.9, 10.55
25000	0.046, 0.142	949, 2124	2.65, 8.16
30000	0.022, 0.096	492, 1574	1.26, 5.52
35000	0.006, 0.066	145, 1179	0.34, 3.77
40000	0.023	466	1.32

Ceiling for Hermes is limited by thrust for the first climb phase. Around 37,000 ft the engines do not produce enough thrust to continue climbing. On the return trip, the engines have sufficient thrust for flight at 45,000 ft above sea level. This illustrates the large change in weight for a successful mission, start to finish.

12.3 Performance Summary

Overall, Hermes met all performance requirements for the main mission. Details of the trans-oceanic ferry mission still need to be better hashed out. For example, cruise altitude, an in-flight refueling schedule, and even geometric modifications to Hermes are items that deserve better attention in order to optimize the performance. The main details of Hermes are compared to current aircraft of similar strategic role in Table 12-3.

Table 12-3: Comparator Aircraft

	Hermes	Antonov AN-72 ¹²⁻⁴	Boeing C-17 ¹²⁻⁵
Max Payload (lbs)	60000	30750	170900
TO Distance (ft)	2432	3055	7740
LDG Distance (ft)	2477	1525	3000
Range (nm)	1200	1240	2762
Cruise Mach	0.80	0.537	0.75
Service Ceiling (ft)	37000 est	35100	45000
TOGW (lbs)	182820	72750	585000
W/S (lb/ft²)	71.1	71.62	154
T/W	0.4	0.92	0.253
LE Wing Sweep	21°	25°	25°
S_{HT}/S_{Wing}	0.282	0.2 est.	0.222
S_{VT}/S_{Wing}	0.22	0.15 est.	0.1 est.
High Lift Systems	USB engine config., fowler flaps	exhaust efflux over upper wing; coanda effect	fixed vane, double slotted flaps
Max Fuel Fraction	0.34	0.392	0.3
Max Payload Fraction	0.328	0.423	0.314
Number of Engines	2	2	4
Type of Engines	high-bypass-ratio turbofan	high-bypass-ratio turbofan	turbofan
Config. of Engines	lower wing mount cantilever T-tail, aft sweep	inboard upper wing mount cantilever T-tail, swept backwards	lower wing pylon mount, in pods cantilever T-tail, swept backwards
Config. of Tail			
Aspect Ratio	8.9	10.3	7.165

Hermes reaches a high level of performance and efficiency during the entire 3 hours it takes to complete its design mission. Its main parameters are noted and summarized in Table 12-4.

Table 12-4: Hermes' Performance Summary

Mission Segment	Weight, lbs	Distance	Mach	L/D	L/D_{target}
TakeOff1	182,000	2432 ft	0.171	~15.5	11
Climb1	179,100	107 nm	0.47 - 0.60	9 - 18.7	16.2
Cruise1	171,000	393 nm	0.8	~13.2	18.3
Mission1	164,500	100 nm	0.6	~6.5	18.1
Landing1	162,700	2477	0.107	~15	10
TakeOff2	101,400	1978 ft	0.171	~15.5	11
Mission2	97,800	100 nm	0.6	~3.9	18.5
Climb2	95,100	38 nm	0.8	5.6 - 16.75	16.5
Cruise2	88,300	462 nm	0.47 - 0.54	~7.9	18.5
Landing2	85,300	1528 ft	0.107	~15	10

Hermes performs well given the BFL and cruise requirements stated in the RFP. Beyond meeting the requirements, Hermes can do better. One area of improvement is a cruise-altitude schedule, where flying higher will increase the Lift-Drag ratio on the return cruise. As previously stated, Hermes tested well during ferry runs as well, due to its lower overall weight. However, she has not reached her potential.

13 Cost Estimation

The cost of our proposal is not a concern in the RFP. The RFP does not give a ceiling on the cost per aircraft resulting from our design, so the concept will not be thrown out simply because it does not meet an arbitrary limit. However, the cost could not be allowed to get out of hand because the customer will take the cost of the proposal into consideration. It is expected that every proposal to the customer will meet the requirements in the RFP, so costs were kept into consideration to keep the costs from getting too high because it will factor into the customer's decision.

13.1 Flyaway and Life Cycle Cost Estimation

The Modified DAPCA IV Model was used to estimate how much the proposal will cost. This estimation relies mostly on the concept's empty weight, maximum velocity, and the number of aircraft produced. The RFP calls for estimates for 150, 500, and 1500 aircraft, so we used those numbers in our estimations. Other elements that are used in this estimation method are the number of flight-test aircraft produced to test the design, the number of engines used in the design, the engine's maximum thrust and Mach number, the turbine inlet temperature, and the cost of the avionics systems used in the aircraft. The model also incorporates two "fudge factors" into the estimation; one is for the use of new technologies, the other is for our company's profit margin. The values of these input elements and the resulting flyaway cost estimations can be found in the tables below.

Table 13-1: Main Inputs for Flyaway Cost Estimation

Input	Value	Units
Empty Weight	78,720	lb
Maximum Velocity	564	mph
Production Quantity of Aircraft	150/500/1,500*	---
Number of Flight Test Aircraft	4	---
Production Quantity of Aircraft Engines	300/1,000/3,000*	---
Maximum Engine Thrust	32,730	lb
Maximum Engine Mach Number	1	---
Turbine Inlet Temperature	1600	K
Cost of Avionics Per Plane	500,000	\$
Advanced Design Factor	1.2	---
Investment Cost Factor	1.1	---

*As required by the RFP

Table 13-2: Flyaway Cost Estimation

Production Run	Flyaway Cost (in billions)	Flyaway Cost Per Plane (in millions)
150	\$14.381	\$95.879
500	\$28.912	\$57.824
1,500	\$59.650	\$39.767

The Modified DAPCA IV Model gives an estimate of the flyaway costs for the proposal. The RFP also calls for an estimate of the life cycle costs for our design. To get this number, the methods laid out in Roskam were used to estimate both the operational costs and the disposal costs of our design (ref. 27). Again, this is done for possible orders of 150, 500, and 1,500 aircraft. Major considerations for operational costs are the amount of fuel used per mission, the cost of fuel, the number of anticipated flight hours per year, and the number of years the aircraft is anticipated to be in service. The disposal cost is assumed to be one percent of the total life cycle cost. The life cycle cost estimation can be found in the table below.

Table 13-3: Life Cycle Cost Estimation

Production Run	Life Cycle Cost (in billions)	Life Cycle Cost Per Plane (in millions)
150	\$74.471	\$496.471
500	\$229.016	\$458.031
1,500	\$726.290	\$484.913

13.2 Cost Sensitivities

While it is hoped that the sizing and performance numbers are final, it is known that certain situations may arise in which numbers may be forced to change. If these changes are not requested by the customer, then it is expected that Arrowspace would be fined for changing the size, especially the weight, or the performance of the aircraft. Therefore, it was determined that there was a need to study the cost sensitivities to changes in the aircraft's sizing and performance. Specifically, the additional cost of adding 100 lbs to the TOGW and the payload weight as well as adding 100 nm to the aircraft's range was studied. Table 13-4 describes the change requested, the empty weight penalty, and the additional flyaway cost incurred.

Table 13-4: Cost Sensitivities

Change Made/Requested	Empty Weight Penalty (lbs)	Additional Flyaway Cost per Plane
Add 100 lbs to TOGW	44.173	\$39,684
Add 100 lbs to payload	118.67	\$106,602
Add 100 nm to Range	2798.376	\$2,506,663

References

- [1] "C-17 Aircraft Data" *McDonnell Douglas*. January 1992.
- [2] Callister, William., *Fundamentals of Materials: Science and Engineering*, Wiley, 2004.
- [3] Day, Dwayne A. *Slotted Wings, Flaps, and High Lift Devices*. U.S. Centennial of Flight Commission. 2007
<http://www.centennialofflight.gov/essay/Evolution_of_Technology/High_Lift_Devices/Tech6.htm>.
- [4] Drela, Mark and Youngren, Harold. "XFOIL 6.9".
- [5] "GE - Aviation: Commercial." *General Electric Company* 2007.
<http://www.geae.com/engines/commercial/index.html>.
- [6] Gillette, W.B., and Mohn, L.W., and Ridley, H.G., and Nark, T.C., "Upper-Surface Blowing Nacelle Design Study for a Swept Wing Airplane at Cruise Conditions," NASA Paper CR-2427 (1974).
- [7] Gochrane, John A., and Riddle, Dennis W., and Stevens, Victor C., and Shovlini, Michael D., "Selected Results from the Quiet Short-Haul Research Aircraft Flight Research Program," AIAA Paper 81-2625R (1982).
- [8] Grasmeyer, J. LDstab FORTRAN program "Stability and Control Derivative Estimation and Engine-Out Analysis."
- [9] Grotz, Charles A. "Development of the YC-14 Propulsion System." AIAA Paper 75-1314 (1975).
- [10] Etkin, B., and Reid, L. D., *Dynamics of Flight: Stability and Control*, 3rd ed., Wiley, 1996.
- [11] *Flight Research at Ames 1940-1997*. 2007. <<http://history.nasa.gov/SP-3300/sp3300.htm>>.
- [12] *High-Lift Systems*. Quest for Performance: The Evolution of Modern Aircraft. 2007<<http://www.hq.nasa.gov/pao/History/SP-468/ch10-5.htm>>.
- [13] *Jane's All the World's Aircraft*, 92nd ed., New York, Jane's Publishing Co., 2001-2002.
- [14] *Jane's Aircraft of the World.*, New York, Jane's Publishing Co., 2005-2006.
- [15] Jukes, Malcom., *Aircraft display systems.*, AIAA Education Series., AIAA Reston, VA, 2004.
- [16] Kimes, Lucas J., "YC-14 Engine Installation Features," AIAA Paper 74-972 (1974).
- [17] Koenig, D. and Aoyagi, K., "Maximum Lift of Upper Surface Blowing STOL Aircraft with Swept Wings," AIAA Paper 75-868 (1975).
- [18] Kroo, I., "Tail Sizing for Fuel-Efficient Transports," AIAA Paper 83-2476 (1983).
- [19] Lamar, J., "LAMDES".
- [20] Lamar, J. VLMpc FORTRAN program "Vortex Lattice Analysis and Design."
- [21] Lynn, Sean, "Summary Report for an Undergraduate Research Project to Develop Programs for Aircraft Takeoff Analysis in the Preliminary Design Phase," Virginia Tech, 1994.

- [22] MIL-F-8785C
- [23] Marchman, J.F., Intro to Aerodynamics & Aircraft Performance, Virginia Tech, 2004.
- [24] Mason, W. H., “Aircraft Configuration Design Options”, Virginia Tech, 17.
- [25] Mason, W. H., “Drag: An Introduction”, 2007.
- [26] Mason, W. H., “Straight-Line Wrap or Ruled Surface Wing Twist compared to Minimum Drag Twist”, Virginia Tech, 1.
- [27] Mason, W. H., “Wing Planform Geometry Analysis,” January, 2006.
- [28] MASS-Military Airborne Surveillance systems. L-3 Communications, 2006.
<<http://www.acssonboard.com/products/mass/>>.
- [29] Megson, THG., *Aircraft Structures for engineering students*, 3rd ed., Elsevier, New York, 1999.
- [30] Morrow, M., “Aircraft Mission Performance Evaluation: Mission 1.3,” 2002.
- [31] Multifunctional Composite Laboratory. UCLA. 2007
<<http://www.seas.ucla.edu/mcl/references/Hyoungseock/TheMechanicalbehaviorofGLARELaminatesforaircraftstructures.pdf>>.
- [32] Murman, Earll. “Transonic Airfoil Analysis: TSFOIL2”.
- [33] Naghshineh-Pour, Amir. “Structural Optimization and Design of a Strut-Braced Wing Aircraft,” 1998.
- [34] Raymer, D. P., *Aircraft Design: A Conceptual Approach-Fourth Edition*, AIAA Education Series, AIAA, Reston, VA, 2006.
- [35] Riddle, Dennis W. and Stevens, Victor C., “Performance Studies on the Application of Four-Engine and Two-Engine USB Propulsive Lift to the E-2C Aircraft,” AIAA Paper 86-2694 (1986).
- [36] Roskam, J., *Airplane Design Part I*, DAR Co., Lawrence, KS, 2002.
- [37] Roskam, J., *Airplane Design Part II*, DAR Co., Lawrence, KS, 1999.
- [38] Roskam, J., *Airplane Design Part V*, DAR Co., Lawrence, KS, 2002.
- [39] Roskam, J., *Airplane Design Part VI*, DAR Co., Lawrence, KS, 1999.
- [40] Roskam, J., *Airplane Design Part VII*, DAR Co., Lawrence, KS, 2002.
- [41] Roskam, J., *Airplane Design Part VIII*, DAR Co., Lawrence, KS, 2002.
- [42] Roskam, Jan., *Airplane Design Preliminary Configuration Design and Integration of the Propulsion System*, 1st ed. Vol. 2, DAR Co., Lawrence, KS, 1986.
- [43] Scientific Electronic Library. 2007 <<http://www.scielo.br/img/revistas/mr/v9n3/31782t3.gif>>.
- [44] Wimpers, J., and Neberry C., “The YC-14 STOL Prototype: Its Design, Development, and Flight Test,” AIAA Paper, 1998.

- [45] Venik's Aviation. 2007 <<http://www.aeronautics.ru/img002/an70-cutaway-diagram.jpg>>.
- [46] YC-14 Advanced Medium STOL Transport (AMST). Global Security. 2007 <<http://www.globalsecurity.org/military/systems/aircraft/c-14.htm>>.